

## RESEARCH ARTICLE

# The p.E152K-STIM1 mutation deregulates Ca<sup>2+</sup> signaling contributing to chronic pancreatitis

Miguel Burgos<sup>1,2,3,\*</sup>, Reginald Philippe<sup>1</sup>, Fabrice Antigny<sup>4,5,6</sup>, Paul Buscaglia<sup>1,7</sup>, Emmanuelle Masson<sup>1</sup>, Sreya Mukherjee<sup>8</sup>, Pauline Dubar<sup>1</sup>, Cédric Le Maréchal<sup>1</sup>, Florence Campeotto<sup>9</sup>, Nicolas Lebonvallet<sup>10</sup>, Maud Frieden<sup>6</sup>, Juan Llopis<sup>2</sup>, Beatriz Domingo<sup>2</sup>, Peter B. Stathopoulos<sup>11</sup>, Mitsuhiko Ikura<sup>12</sup>, Wesley Brooks<sup>8</sup>, Wayne Guida<sup>8</sup>, Jian-Min Chen<sup>1</sup>, Claude Ferec<sup>1</sup>, Thierry Capiod<sup>13</sup> and Olivier Mignen<sup>1,7,\*</sup>

## ABSTRACT

Since deregulation of intracellular Ca<sup>2+</sup> can lead to intracellular trypsin activation, and stromal interaction molecule-1 (STIM1) protein is the main regulator of Ca<sup>2+</sup> homeostasis in pancreatic acinar cells, we explored the Ca<sup>2+</sup> signaling in 37 STIM1 variants found in three pancreatitis patient cohorts. Extensive functional analysis of one particular variant, p.E152K, identified in three patients, provided a plausible link between dysregulated Ca<sup>2+</sup> signaling within pancreatic acinar cells and chronic pancreatitis susceptibility. Specifically, p.E152K, located within the STIM1 EF-hand and sterile  $\alpha$ -motif domain, increased the release of Ca<sup>2+</sup> from the endoplasmic reticulum in patient-derived fibroblasts and transfected HEK293T cells. This event was mediated by altered STIM1–sarco/endoplasmic reticulum calcium transport ATPase (SERCA) conformational change and enhanced SERCA pump activity leading to increased store-operated Ca<sup>2+</sup> entry (SOCE). In pancreatic AR42J cells expressing the p.E152K variant, Ca<sup>2+</sup> signaling perturbations correlated with defects in trypsin activation and secretion, and increased cytotoxicity after cholecystokinin stimulation.

This article has an associated First Person interview with the first author of the paper.

**KEY WORDS:** STIM1, Pancreatitis, Missense mutation, Modifier variant, Ca<sup>2+</sup> signaling, Trypsin secretion

<sup>1</sup>Université de Brest, INSERM, EFS, UMR 1078, GGB, F-29200 Brest, France.

<sup>2</sup>Centro Regional de Investigaciones Biomédicas (CRIB) and Facultad de Medicina de Albacete, Universidad de Castilla-La Mancha, 02002 Albacete, Spain.

<sup>3</sup>Complejo Hospitalario Universitario de Albacete (UI-CHUA), 02002 Albacete, Spain.

<sup>4</sup>Univ. Paris–Sud, Faculté de Médecine, Université Paris-Saclay, 94270 Le Kremlin Bicêtre, France.

<sup>5</sup>Inserm UMR\_S 999, Hôpital Marie Lannelongue, 92350 Le Plessis Robinson, France. <sup>6</sup>Department of Cell Physiology and Metabolism, Geneva Medical Center, CH-1211 Geneva, Switzerland.

<sup>7</sup>UMR1227, Lymphocytes B et Autoimmunité, Université de Brest, INSERM, CHU de Brest, BP824, F29609 Brest, France.

<sup>8</sup>Department of Chemistry, University of South Florida, Tampa, FL 33620, USA. <sup>9</sup>Hôpital Necker, AP-HP, Service de Gastroentérologie et Explorations Fonctionnelles Digestives Pédiatriques, Paris Descartes-Sorbonne Paris Cité Université, Institut Imagine, 75015 Paris, France.

<sup>10</sup>Laboratory of Interactions Keratinocytes Neurons (EA4685), University of Western Brittany, F-29200 Brest, France. <sup>11</sup>Department of Physiology and Pharmacology, Schulich School of Medicine and Dentistry, London, ON N6A 5C1, Canada.

<sup>12</sup>Department of Medical Biophysics, University of Toronto, Princess Margaret Cancer Centre, University Health Network, Toronto, ON M5G 2M9, Canada.

<sup>13</sup>INSERM Unit 1151, Institut Necker Enfants Malades (INEM), Université Paris Descartes, Paris 75014, France.

\*Authors for correspondence (Mburoslozano@sescam.jccm.es; olivier.mignen@univ-brest.fr)

© M.B., 0000-0001-6674-0798; J.-M.C., 0000-0002-2424-3969; O.M., 0000-0001-7913-6119

Handling Editor: John Heath

Received 24 January 2020; Accepted 24 December 2020

## INTRODUCTION

Cell damage observed in experimental acute pancreatitis results in part from abnormal intracellular Ca<sup>2+</sup> concentrations ([Ca<sup>2+</sup>]<sub>i</sub>) (Petersen, 2009; Gerasimenko et al., 2014). Elevated [Ca<sup>2+</sup>]<sub>i</sub> signals can be elicited by combinations of fatty acids, alcohol or bile acids, leading to the appearance of fatty acid ethyl esters, which mediate the toxic alcohol effects on pancreatic acinar cells. This higher [Ca<sup>2+</sup>]<sub>i</sub> results from the excessive release of endoplasmic reticulum (ER) Ca<sup>2+</sup> stores or from an increase in Ca<sup>2+</sup> influx such as store-operated Ca<sup>2+</sup> entry (SOCE) regulated by stromal interaction molecule-1 (STIM1) and mediated by Orai1 proteins. The sustained Ca<sup>2+</sup> signals and cytosolic Ca<sup>2+</sup> overload contribute to the development of acute pancreatitis (Gerasimenko et al., 2009; Lur et al., 2011; Wen et al., 2015) through initiating activation of intracellular proteases responsible for cell autodigestion (Raraty et al., 2000; Gerasimenko et al., 2013; Zhu et al., 2018). Consistent with this, the inhibition of Ca<sup>2+</sup> channel activity has been described as protective in pancreatitis and represents a therapeutic option (Son et al., 2019; Waldron et al., 2019).

STIM1 is a single-pass transmembrane protein mainly localized to the ER membrane and has been established as the main ER Ca<sup>2+</sup> sensor in non-excitabile and excitabile cells (Yuan et al., 2009). The EF-hand and sterile  $\alpha$ -motif (EF-SAM) domains of STIM1 are located in the luminal region of the ER and, together, act as a Ca<sup>2+</sup> sensor to initiate SOCE activation. After ER Ca<sup>2+</sup> store depletion, STIM1 oligomerizes and subsequently translocates to ER–plasma membrane junctions (Liou et al., 2005; Roos et al., 2005) allowing interaction with store-operated Ca<sup>2+</sup> channels (Wu et al., 2006; Park et al., 2009; Nwokonko et al., 2017). The association between *STIM1* gene variants and the development of different diseases has been elucidated. Among them, we can find *STIM1* variants driving to loss of function in autoimmunity and immunodeficiencies like E136X (Picard et al., 2009) and homozygous p.L74P and p.L374P (Parry et al., 2016; Vaeth et al., 2017), or reporting a gain of function like p.D84G/p.H84N/p.H109R for tubular-aggregate myopathy (Böhm et al., 2013), p.R304W for Stormorken syndrome (Misceo et al., 2014; Morin et al., 2014; Nesin et al., 2014), p.I115F (Hedberg et al., 2014) and p.D84E (Noury et al., 2017) for tubular-aggregate myopathy, and p.S88G/p.R304Q for neuromuscular malfunctions (Harris et al., 2017). The importance of Ca<sup>2+</sup> signaling for the regulation of pancreatic zymogen activation and the key role of STIM1 in this process suggests that variants in the *STIM1* gene may also contribute to chronic pancreatitis by disturbing Ca<sup>2+</sup> homeostasis within the pancreatic tissue. In this regard, Sofia and colleagues have recently analyzed the *STIM1* in 80 patients with idiopathic chronic pancreatitis (ICP) and found three missense mutations in different patients (Sofia et al., 2016). Indeed, a recent genetic study of the Ca<sup>2+</sup> channel TRPV6 in pancreatitis cohorts described variants of the



was significantly increased in cells expressing STIM1 p.A38P and p.E152K compared to WT STIM1-expressing cells (Fig. 1B,C). We observed the same effect after tert-Butylhydroquinone (tBHQ) addition with respect to STIM1 p.E152K by comparison with WT STIM1-expressing cells (Fig. S1A).

The p.E152K variant was of particular interest for three reasons. First, it was observed in three patients but not in controls (Masson et al., 2019, preprint). It should also be pointed out that p.E152K is extremely rare in the general population; its average allele frequency in gnomAD (gnomad.broadinstitute.org/) was 0.0001162 (30/258080; as of November 30, 2018). Second, p.E152K affects a highly conserved amino acid of the EF-SAM domain located within the seventh  $\alpha$ -helix (Fig. S1B). The highly conserved EF-SAM domain is central to STIM1 oligomerization (Stathopoulos et al., 2006). Gain-of-function variants in the EF-hand domain have been previously reported to induce constitutive STIM1 oligomerization and have been associated with tubular-aggregate myopathy (Böhm et al., 2013; Hedberg et al., 2014; Lacruz and Feske, 2015). Third, and somewhat intriguingly, all three patients harboring the *STIM1* p.E152K variant were found to harbor heterozygous variants in other known chronic pancreatitis susceptibility genes. Thus, of the two French patients, one harbored *PRSSI* p.N29I whereas the other harbored *PRSSI* p.P36R. Both *PRSSI* p.N29I and *PRSSI* p.P36R are rare variants whereas *PRSSI* p.N29I is a well-known pathogenic mutation; *PRSSI* p.P36R is currently classified as benign (see the Genetic Risk Factors in Chronic Pancreatitis Database; <http://www.pancreasgenetics.org/index.php>). In the Chinese patient harboring the *STIM1* p.E152K variant, the situation is more complicated; the patient also harbored the *SPINK1* c.194+2T>C variant, the *PRSSI* c.623G>C (p.G208A) variant and the *CTRC* c.180C>T (p.G60=) variant. All three of the latter variants have been recently shown to be associated with chronic pancreatitis in a large Chinese cohort study (Zou et al., 2018).

In view of the aforementioned points, we focused our functional exploration on the p.E152K variant.

### Ca<sup>2+</sup> signaling deregulation in fibroblasts obtained from an ICP patient harboring the p.E152K variant

Fibroblasts were obtained from the patient carrying the *STIM1* p.E152K variant and the *PRSSI* p.P36R variant (II.2), his mother who harbored neither of the two variants (I.2) and his brother (II.1) carrying only the *PRSSI* p.P36R variant (Fig. 2A). Clear and significant increases in the speed and amplitude of the ER Ca<sup>2+</sup> release as well as the SOCE rate were observed in fibroblasts from the patient as compared to the two aforementioned relatives (Fig. 2B).

### Modulation of ER Ca<sup>2+</sup> homeostasis in HEK293T cells expressing the p.E152K variant

To further explore the role of the p.E152K variant, we performed experiments in HEK293T cells expressing different plasmids containing WT STIM1, STIM1-E152K or empty vector (Fig. S1C). One possible explanation for the increased ER Ca<sup>2+</sup> release is enhanced passive Ca<sup>2+</sup> leakage from the ER when TG blocks SERCA. However, receptor-mediated Ca<sup>2+</sup> release consequent to the activation of InsP<sub>3</sub> receptors (InsP<sub>3</sub>Rs) following carbachol (CCh) stimulation (Fig. 3A; Fig. S1D, left panel) or ATP (Fig. 3B; Fig. S1D, right panel) is also significantly enhanced. A series of p.E152K, p.E152D, p.E152V, p.E152Q and p.E152R variants introduced into STIM1 confirmed the key role of the negative charge contributed by this basic amino acid in relation to the enhanced ER Ca<sup>2+</sup> release phenotype (Fig. S1E). For example, p.E152R shows the same ER Ca<sup>2+</sup> increase as p.E152K.

Next, we directly monitored changes in ER Ca<sup>2+</sup> concentration in HEK293T cells transfected with the ER-targeted cameleon probe D1ER (a Ca<sup>2+</sup> sensor) (Palmer et al., 2004). ER Ca<sup>2+</sup> concentration ([Ca<sup>2+</sup>]<sub>ER</sub>) was determined after D1ER titration (Fig. S1F) as

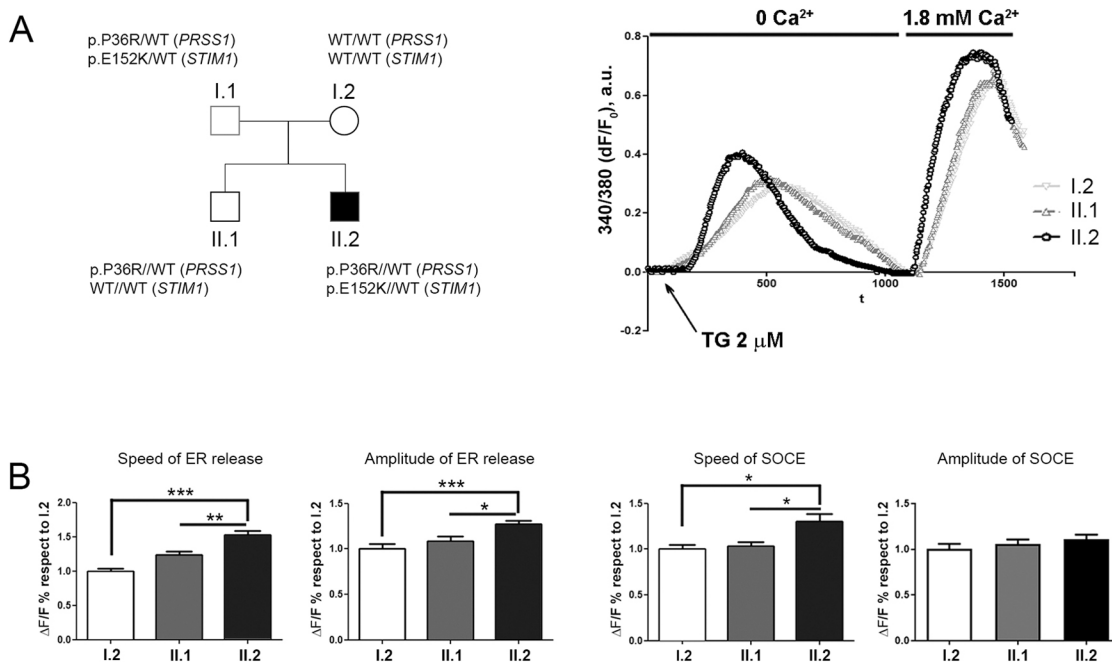


**Fig. 2. Analysis of Ca<sup>2+</sup> responses to TG in fibroblasts isolated from a chronic pancreatitis patient harboring the *STIM1* p.E152K variant.** (A) Left panel, family tree of the patient II.2. *STIM1* genotypes are given for each family member. Right panel, representative traces of TG-evoked Ca<sup>2+</sup> transients in Fura-2-loaded fibroblasts from patient II.2 and two of his relatives (I.2 and II.1). (B) Mean  $\pm$  s.e.m. values of the rate and amplitude of ER Ca<sup>2+</sup> release and SOCE normalized to I.2 parameter values.  $n=94$  (I.2 and II.1) and 134 (II.2). \* $P<0.05$ ; \*\* $P<0.001$ ; \*\*\* $P<0.0005$  (ANOVA with Tukey's post hoc test).

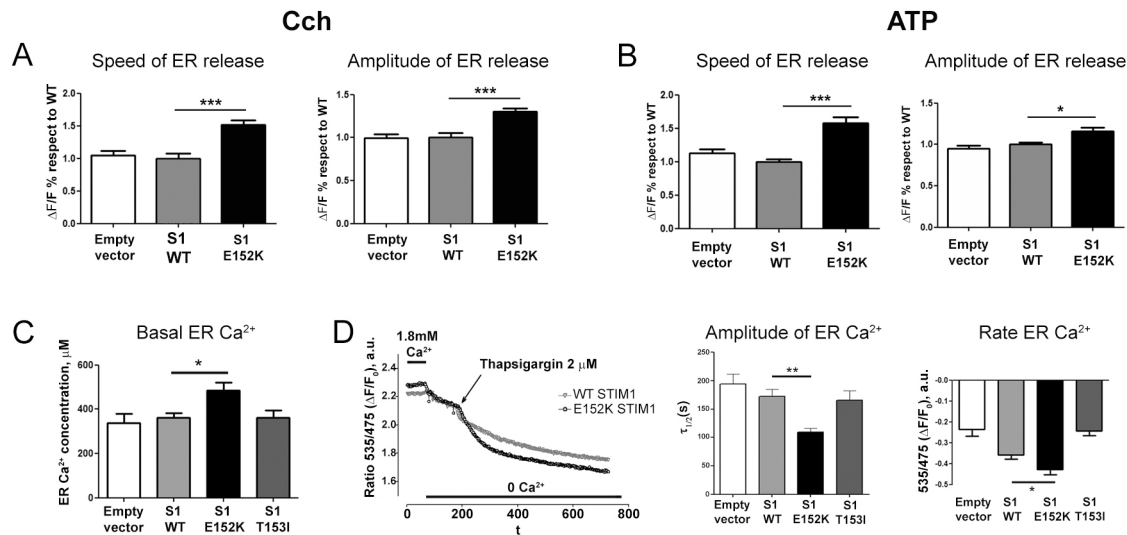


**Fig. 3. Analysis of the  $\text{Ca}^{2+}$  response in HEK293 cells expressing either WT or mutated STIM1.** (A) Mean $\pm$ s.e.m. values of the speed (left panel) and amplitude (right panel) of ER  $\text{Ca}^{2+}$  release after 100  $\mu\text{M}$  CCh treatment in the absence of extracellular  $\text{Ca}^{2+}$ . Three independent experiments with at least 30 cells per experiment were performed for each condition. (B) Mean $\pm$ s.e.m. values of the speed (left panel) and amplitude (right panel) of ER  $\text{Ca}^{2+}$  release after 100  $\mu\text{M}$  ATP treatment in the absence of extracellular  $\text{Ca}^{2+}$ . Three independent experiments with at least 30 cells per experiment were performed for each condition. (C) Basal  $[\text{Ca}^{2+}]_{\text{er}}$  ( $\mu\text{M}$ ) evaluated using the D1ER probe and values normalized based on the calibration curve. Results are mean $\pm$ s.e.m. Three independent experiments with at least 30 cells per experiment were performed for each condition. (D) Representative traces of  $[\text{Ca}^{2+}]_{\text{er}}$  variation after addition of 1  $\mu\text{M}$  TG ( $\text{Ca}^{2+}$ -free medium) to D1ER-transfected HEK293T cells expressing WT STIM1 or E152K STIM1 (left hand panel). Center panel, quantification of the ER  $\text{Ca}^{2+}$  release rate ( $t_{1/2}$ ) in cells expressing WT STIM1, E152K STIM1, T153I STIM1 or empty vector. Right hand panel, quantification of the amplitude of  $[\text{Ca}^{2+}]_{\text{ER}}$  release after TG (1  $\mu\text{M}$ ) treatment in cells expressing WT STIM1, E152K STIM1, T153I STIM1 or empty vector,  $n=42$  (empty vector), 106 (WT), 76 (E152K) and 54 (T153I). Results are mean $\pm$ s.e.m. \* $P<0.05$ ; \*\* $P<0.001$ ; \*\*\* $P<0.0005$  (ANOVA with Tukey's post hoc test).

previously described (Shen et al., 2011). The simplest explanation for the increase in ER  $\text{Ca}^{2+}$  release is that a higher  $[\text{Ca}^{2+}]_{\text{er}}$  enhances the driving force for the ER  $\text{Ca}^{2+}$  efflux. No significant increase in  $[\text{Ca}^{2+}]_{\text{er}}$  was observed when overexpressing WT STIM1 or STIM1-T153I (Fig. 3C). However, the ER  $\text{Ca}^{2+}$  concentration was markedly increased in cells expressing STIM1-E152K as compared to WT STIM1 (Fig. 3C, 484 versus 363  $\mu\text{M}$ ,  $P<0.05$ ). After blocking SERCA using TG, a significant enhancement ( $P<0.001$ ) of both the rate (36%) and amplitude (23%) of  $[\text{Ca}^{2+}]_{\text{er}}$  decrease was only observed in STIM1-E152K-expressing cells (Fig. 3D). Finally, one question that was unresolved was why the ER  $\text{Ca}^{2+}$  release led to an increase in SOCE in fibroblasts bearing the p.E152K variant, while this effect was not observed in HEK293T cells. According to literature (Liao et al., 2008), STIM1 overexpression in HEK293T cells is not sufficient to increase SOCE amplitude unless ORAI1 is co-transfected at the same time. Therefore, we performed a double STIM1-ORAI1 transfection, which resulted in an increase in both ER release and SOCE in cells expressing STIM1-E152K referred to WT (Fig. S1G).

#### p.E152K-STIM1 expression modulates ER $\text{Ca}^{2+}$ refilling by changing SERCA conformation

An increase in SERCA pump activity would explain the increase in  $[\text{Ca}^{2+}]_{\text{er}}$  and  $\text{Ca}^{2+}$  efflux in cells expressing STIM1-E152K. SERCA pump activity, estimated by quantifying ER  $\text{Ca}^{2+}$  refilling following store depletion with tBHQ in permeabilized and non-permeabilized D1ER-expressing cells (Fig. 4A,B), is clearly enhanced in STIM1-E152K-expressing cells independently of SOCE as demonstrated by experiments performed under permeabilizing conditions.

Hence, we hypothesized that SERCA activity can be regulated by STIM1. Different studies have reported the interaction of STIM1 with SERCA2 and SERCA3 pumps (López et al., 2008; Sampieri et al., 2009; Manjarrés et al., 2010). Different fluorescence resonance

energy transfer (FRET)-based SERCA constructs that indicate the conformational state of SERCA have been developed, which function by measuring FRET between fluorescent proteins fused to its cytoplasmic domains (Satoh et al., 2011; Hou et al., 2012; Pallikkuth et al., 2013). By using one of these constructs, RG-SERCA, we sought to establish whether the stronger association between SERCA and STIM1-E152K could modulate SERCA conformational state changes. At rest, a basal FRET level is seen, whereas after tBHQ addition, the FRET signal decreases as the SERCA cytoplasmic headpiece is driven to an 'opened' conformation (Hou et al., 2012). Remarkably, we observed a reduction in the basal FRET-to-GFP ratio (FRET/GFP) in cells overexpressing WT STIM1 in comparison to empty vector, and an even lower ratio in cells expressing E152K-STIM1 (Fig. 4C). After tBHQ addition, the amplitude and rate of SERCA conformational change is higher in E152K-expressing cells than WT. The maximal rate of FRET/GFP decrease induced by  $\text{Ca}^{2+}$  store release was significantly enhanced in cells expressing STIM1-E152K. In terms of amplitude, both WT STIM1 and STIM1-E152K diminished the FRET/GFP decrease induced by tBHQ, E152K having a stronger effect. When ER  $\text{Ca}^{2+}$  was depleted, SERCA displayed a more rapid conformational change in the presence of STIM1-E152K in comparison to WT STIM1, although smaller in amplitude.

To reinforce our hypothesis of a modification of STIM1-SERCA interaction in the presence of the E152K variant, we performed immunoprecipitation experiments. SERCA and STIM1 co-immunoprecipitate under resting conditions and an increase in SERCA-STIM1 association was observed in STIM1-E152K-expressing cells as compared to cells expressing WT STIM1 (Fig. S2A). The western blot in Fig. S2B shows the similar overexpression of WT STIM1 and STIM1-E152K in this experiment. These results suggest that, under resting  $[\text{Ca}^{2+}]_{\text{er}}$  conditions, a fraction of STIM1 is already associated with SERCA.

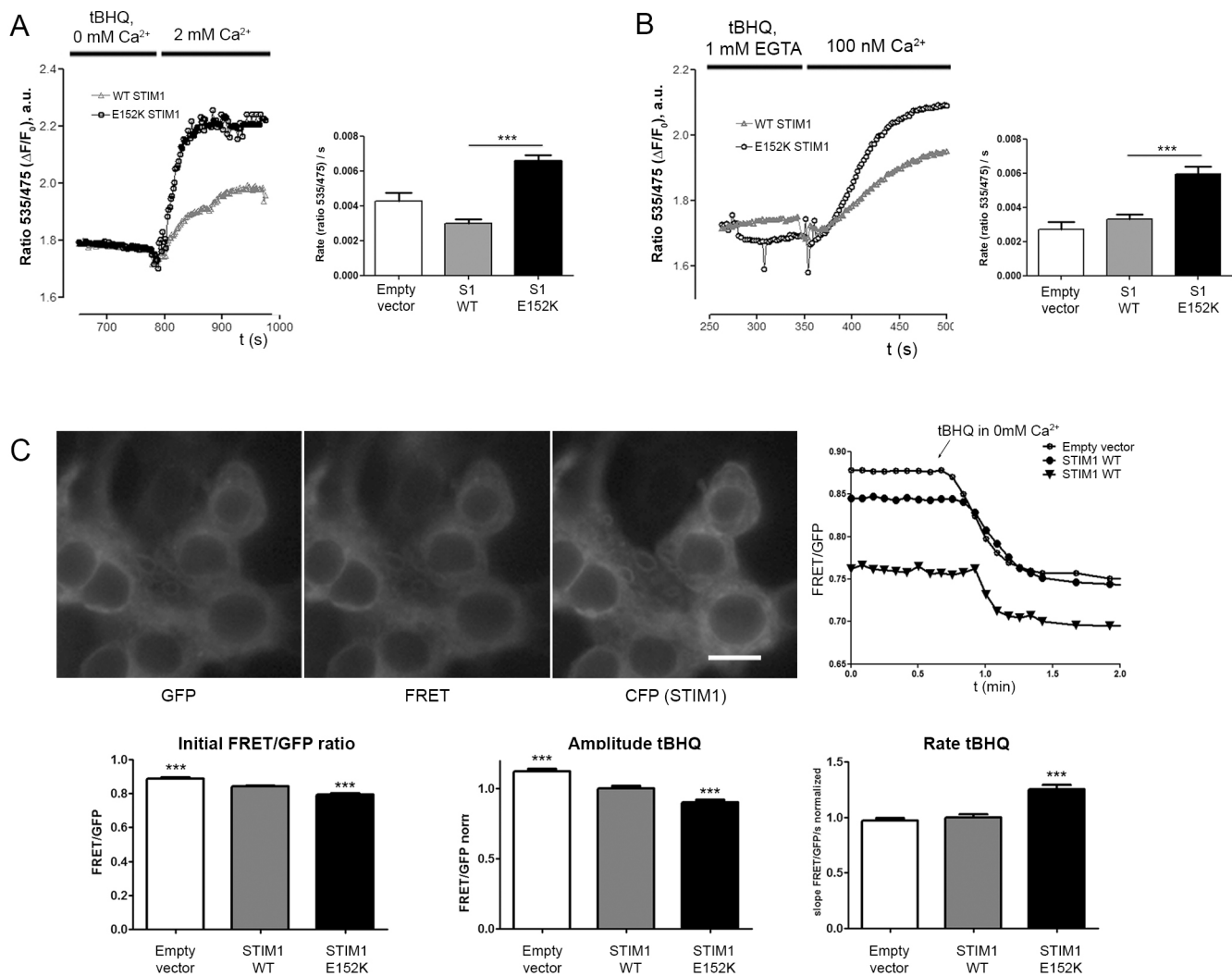


**Fig. 4. STIM1–SERCA modification induced by the E152K variant.** (A,B) Cells were transfected with either WT or E152K STIM1. ER Ca<sup>2+</sup> changes were evaluated in cells transfected with ER-targeted cameleon probe D1ER. In A, ER Ca<sup>2+</sup> depletion was induced by 15  $\mu$ M tBHQ, and ER Ca<sup>2+</sup> refilling was evaluated by changing the Ca<sup>2+</sup>-free extracellular medium using a solution containing 1.8 mM Ca<sup>2+</sup> (representative traces in left hand panel) and quantification of the ER Ca<sup>2+</sup> refilling rate in cells expressing WT STIM1, E152K STIM1 or an empty vector (right hand panel). Results are mean $\pm$ s.e.m.  $n=19$  (empty vector), 67 (WT) or 46 (E152K) (right hand panel). In B, the quantification of ER Ca<sup>2+</sup> refilling rate in cells expressing WT STIM1, E152K STIM1 or an empty vector was performed under permeabilizing conditions. Left hand panel shows representative traces of ER Ca<sup>2+</sup> variations in cells permeabilized by 60  $\mu$ M digitonin and after addition of 15  $\mu$ M tBHQ. ER Ca<sup>2+</sup> refilling was induced by addition of 100 nM Ca<sup>2+</sup>. Results are mean $\pm$ s.e.m.  $n=8$  (empty vector), 91 (WT) or 71 (E152K) (right hand panel). (C) Left, images of HEK293 cells showing a double transfection FRET-based intramolecular SERCA construct (RG-SERCA, GFP-tagRFP) and STIM1 WT–CFP. Scale bar: 50  $\mu$ m. Graph on right of images shows the basal FRET/GFP fluorescence ratio level, which decreases as the SERCA adopts an open conformation after tBHQ addition (right panel). Histograms below show the quantification of differences in basal FRET/GFP ratio (left), amplitude of tBHQ response (center) and rate of tBHQ response (right). Results are mean $\pm$ s.e.m. Three independent experiments with at least 30 cells per experiment were performed for each condition. \*\*\* $P<0.0005$  (ANOVA with Tukey's post hoc test).

Taken together, these data suggest that the p.E152K variant modifies the degree of association between SERCA and STIM1. Among other explanations, the greater STIM1-E152K association with SERCA before store depletion could favor an intermediate cytoplasmic conformational state that responds faster after Ca<sup>2+</sup> depletion.

#### Intrinsic biophysical properties of STIM1-E152K

It is now well established that the EF-SAM domain plays a critical role in the regulation of STIM1 oligomerization (Stathopoulos et al., 2006). Computational modeling of STIM1 for both the WT and the p.E152K variant to discern possible changes in the mutated STIM1 structure (see section on ‘Note on computational modeling of the E152K mutant’ in the Materials and Methods section and

Fig. S3A–C) suggest that a difference in local charge due to the p.E152K mutation may affect STIM1 protein–protein interactions. Using a FRET approach, we observed a difference in FRET multimerisation between WT and E152K mutated STIM1. We observed a significantly higher FRET level between CFP–STIM1-E152K and YFP–STIM1-E152K by comparison with the CFP–WT STIM1 and YFP–WT STIM1 constructs, consistent with an increased efficiency of STIM1-E152K homo-oligomerization (Fig. 5A). FRET analysis of multimerization between WT-STIM1 and STIM1-E152K as expected in a heterologous expression condition, is not relevant due to the higher homo-oligomerization efficiency of mutated STIM1 compared to WT STIM1.

Biophysical analyses were then performed on purified EF-SAM domains of WT or mutated human STIM1 (Fig. S3D). Far-UV

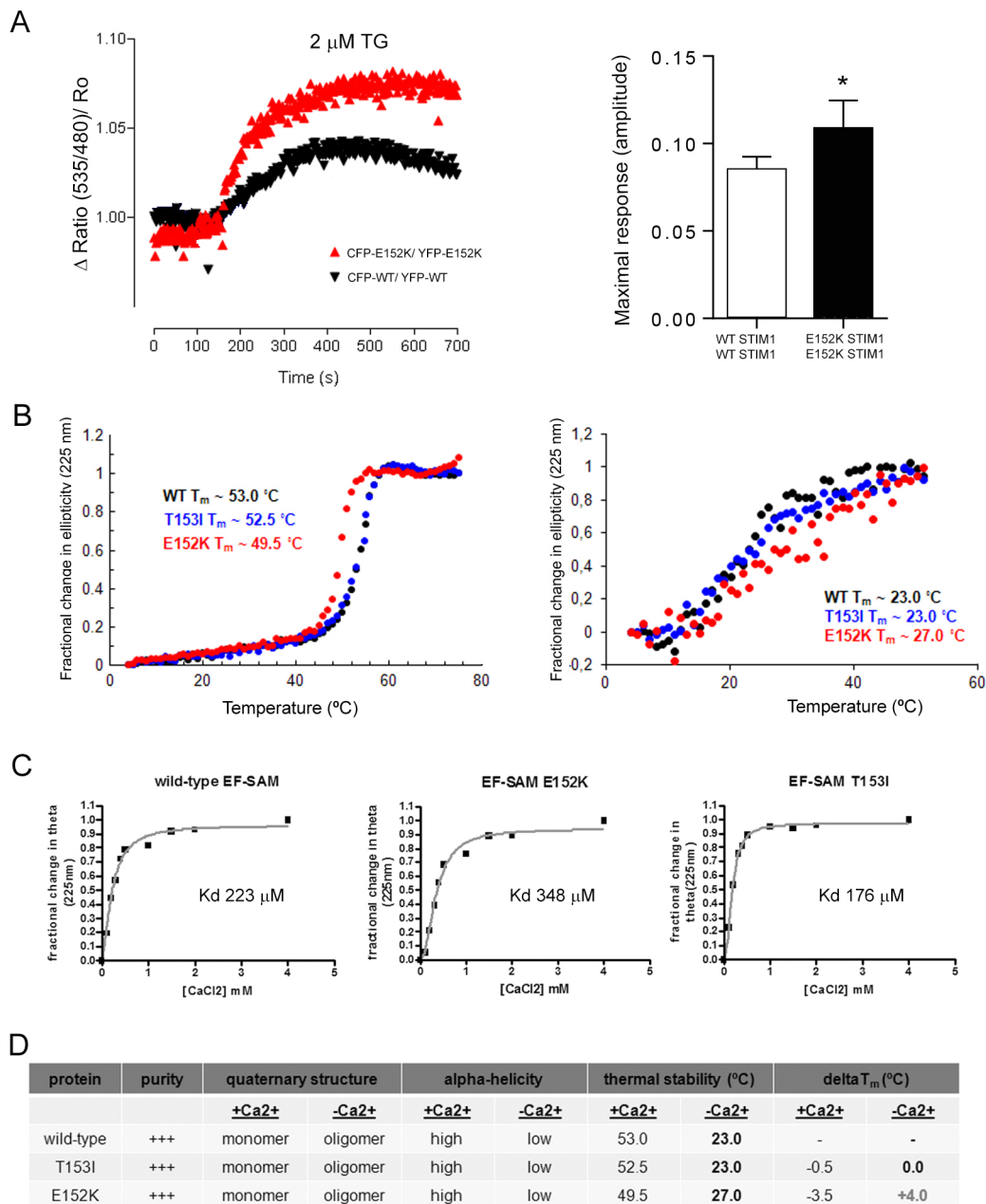


**Fig. 5. Experiments on the biophysical properties of STIM1-E152K.** (A) Left, representative traces of changes in FRET signal (CFP–STIM1 WT/YFP–STIM1 WT, and CFP–STIM1 E152K/YFP–STIM1 E152K) were measured in transfected HEK cells after addition of 1  $\mu\text{M}$  TG to induce ER  $\text{Ca}^{2+}$  store depletion. Right, quantification of maximal FRET amplitude among the different CFP/YFP combinations. Results are mean  $\pm$  s.e.m.  $n=55$  (WT CFP/WT YFP) and 50 (E152K CFP/E152K YFP).  $*P<0.05$  (unpaired two-tailed Student's  $t$ -test). (B) Thermal stability of WT and mutant EF-SAM domains. Thermal stabilities of WT EF-SAM (black circles), T153I EF-SAM (blue circles) and E152K EF-SAM (red circles) domains in the presence (left) and absence (right) of 5 mM  $\text{CaCl}_2$  were estimated from the changes in far-UV-CD at 225 nm as a function of temperature. The apparent midpoint of temperature denaturation ( $T_m$ ) was defined as the temperature where the fractional change in ellipticity was 0.5. Protein concentrations were 10  $\mu\text{M}$  and 40  $\mu\text{M}$  in the  $\text{Ca}^{2+}$ -loaded and -depleted states, respectively. (C)  $\text{Ca}^{2+}$ -binding affinity estimates of WT and mutant EF-SAM domains. Binding curves of 40  $\mu\text{M}$  protein were acquired as the fractional change in ellipticity as a function of  $\text{CaCl}_2$  concentration at 20  $^{\circ}\text{C}$ . Data were fitted to the Hill equation, assuming a negligible effect of protein concentration on the dissociation constant ( $K_d$ ) since  $[\text{protein}] = K_d$ . Buffers in B and C were 20 mM Tris-HCl pH 8, 150 mM NaCl. (D) Summary of WT and mutant EF-SAM biophysical characteristics.

circular dichroism (CD) experiments confirmed that the mutant EF-SAM domains retain the ability to sense  $\text{Ca}^{2+}$  changes through a marked alteration in structure, consistent with the ability of full-length STIM1-E152K to signal SOCE after ER  $\text{Ca}^{2+}$  store depletion (Fig. S3E). Thermal stability studies of the EF-SAM domains revealed that the E152K variant destabilized the  $\text{Ca}^{2+}$ -bound EF-SAM structure ( $T_m$  WT=53  $^{\circ}\text{C}$  versus  $T_m$  E152K=49.5  $^{\circ}\text{C}$ ;

Fig. 5B, left). In contrast, the E152K variant appeared to stabilize the  $\text{Ca}^{2+}$ -depleted EF-SAM structure ( $T_m$  WT  $\sim$ 23  $^{\circ}\text{C}$  versus  $T_m$  E152K  $\sim$ 27  $^{\circ}\text{C}$ ; Fig. 5B, right), with the caveat that both the WT and E152K data showed a high variability due to the overall instability. These results suggest that the enhanced multimerization displayed by STIM1-E152K as compared to WT may be due to the destabilized  $\text{Ca}^{2+}$ -loaded state, which more readily undergoes a

transition to the oligomerization-prone  $\text{Ca}^{2+}$ -depleted state and/or a modified  $\text{Ca}^{2+}$ -depleted state with enhanced oligomer stability.

Size exclusion chromatography with in-line multiangle light scattering (SEC-MALS) allowed us to conclude that in the presence of  $\text{Ca}^{2+}$ , E152K EF-SAM exists primarily as a monomer, but undergoes a shift in the self-association equilibrium towards dimers and oligomers in the absence of  $\text{Ca}^{2+}$  as observed for WT STIM1 and T153I EF-SAM (Fig. S3F). No significant change in the  $\text{Ca}^{2+}$  binding affinity of E152K STIM1 was observed and the measured affinities were in the same range as those previously reported for WT STIM1 EF-SAM (Stathopoulos et al., 2006) (Fig. 5D). Taken together, these data suggest that the E152K EF-SAM variant displays WT-like  $\text{Ca}^{2+}$  sensitivity characteristics in terms of  $\text{Ca}^{2+}$  binding, secondary structure and oligomerization. However, changes in the stability of STIM1 E152K EF-SAM with and without  $\text{Ca}^{2+}$  may contribute to aberrant ER  $\text{Ca}^{2+}$  homeostasis and differences in STIM1 protein interactions. The biophysical properties of the different EF-SAM domains are summarized in Fig. 5D.

### Functional consequences of E152K STIM1 in rat pancreatic acinar cells

In order to probe the physiological consequences of STIM1-E152K expression with a view to potentially linking the observed defects in  $\text{Ca}^{2+}$  signaling to pancreatitis, we next evaluated, in rat pancreatic AR42J cells, the effects of the STIM1 p.E152K variant on  $\text{Ca}^{2+}$  signaling, trypsin activation, trypsinogen secretion and the subsequent consequences for cell fate. As observed in HEK293T cells, a significant increase in the rate and amplitude of ER  $\text{Ca}^{2+}$  release induced by agonist stimulation with cholecystokinin (CCK) (Fig. 6A) or Cch (Fig. S4A) or by TG (Fig. S4B) was obtained in AR42J cells expressing STIM1-E152K (Fig. S4C).

Intra-acinar activation of zymogens is a key event in the initiation of acute pancreatitis (Krüger et al., 2000), and the increased  $\text{Ca}^{2+}$  mobilization observed in STIM1-E152K-expressing cells may lead to an increase in intracellular trypsin activation after stimulation. Trypsin activation was monitored before and after CCK stimulation using the BZiPAR probe (Raraty et al., 2000), which allowed us to detect constitutive activation of trypsin in AR42J cells, which was enhanced following CCK stimulation in a time-dependent manner (Fig. 6B) but was prevented by pretreatment with benzamidine, a competitive inhibitor of trypsin (Fig. S4D). A higher amount of basal activated trypsin, as well as a significant enhancement of trypsin activation after 4 h stimulation, was detected in AR42J cells expressing STIM1-E152K as compared to WT STIM1 or empty vector (Fig. 6B) (12% increase in basal trypsin activity and 49% increase after 4 h CCK treatment, respectively;  $P < 0.001$ ).

Another explanation proposed for cell degradation observed in pancreatitis is a decrease in  $\text{Ca}^{2+}$ -dependent trypsinogen secretion (Gerasimenko et al., 2014). Trypsin cellular content and exocytosis were evaluated as previously described by western blotting of cell lysates and in conditioned medium after CCK treatment of AR42J cells expressing trypsin-1 (PRSS1) (Kereszturi and Sahin-Tóth, 2009). An enhancement of intracellular trypsin and a decrease in trypsin secretion was observed in cells expressing STIM1-E152K as compared to cells transfected with WT STIM1 in this experiment after CCK treatment, suggesting a difference in trypsin secretion when the E152K variant was present (Fig. 6C). In agreement with these findings, the basal level of toxicity was higher in cells expressing STIM1-E152K as compared to cells transfected with an empty vector, WT STIM1 or STIM1-T153I (Fig. 6D). An enhancement of cell toxicity following CCK stimulation was observed in AR42J cells expressing STIM1-E152K in comparison

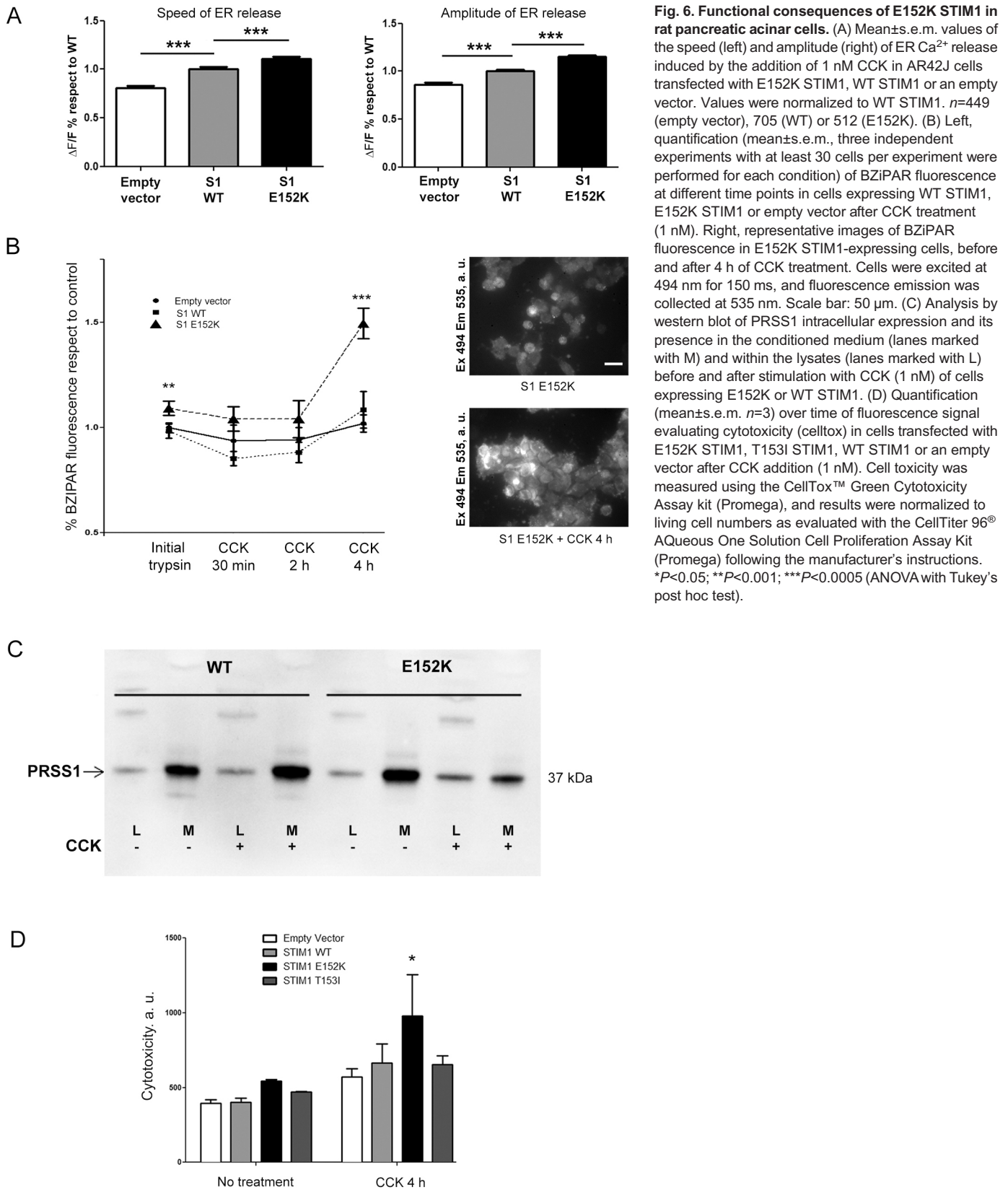
to WT STIM1, in agreement with the increase in trypsin autoactivation observed under the same conditions (Fig. 6B).

### DISCUSSION

It is broadly recognized that early trypsin activation within the pancreatic acinar cells leads to cell necrosis due to protein degradation and is one of the major causes of pancreatitis. Works from Petersen and colleagues (Gerasimenko et al., 2009; Raraty et al., 2000) show the dependence of formation and activation of trypsinogen on  $\text{Ca}^{2+}$  signaling. Since STIM1 is the main ER  $\text{Ca}^{2+}$  sensor in non-excitable cells and a key regulating protein in SOCE, we therefore decided to explore STIM1 polymorphisms in CP cohorts. The importance of STIM1 in physiological processes has been clearly established, as well as implication of its mutations in pathologies (Böhm et al., 2013; Hedberg et al., 2014; Picard et al., 2009). Notably, none of the identified 37 rare *STIM1* variants identified in the three pancreatitis patients cohorts correspond to those previously reported to cause or predispose to other diseases (Lacruz and Feske, 2015), potentially strengthening the notion of the tissue-specific effects of different *STIM1* variants. However, functional screening of these variants in relation to the speed and amplitude of  $\text{Ca}^{2+}$  release from ER stores and SOCE failed to reveal any enrichment of functional variants in patient. This may reflect a common challenge that we face in the functional annotation of disease-predisposing or modifying variants that may either only subtly affect gene expression or protein structure and function, or alternatively may exert their effects in tissue- or cell type-dependent fashion. Nonetheless, extensive functional analysis of one particular variant, p.E152K, which was found in three patients (two French and one Chinese) but not in any of the 3322 controls, established a plausible link between dysregulated  $\text{Ca}^{2+}$  signaling within the pancreatic acinar cells and chronic pancreatitis susceptibility. Since all three patients harboring the *STIM1* p.E152K variant also harbored variants in known chronic pancreatitis susceptibility genes in the trypsin-dependent pathway, the *STIM1* p.E152K variant may be acting as a disease modifier.

E152K is located in the EF-SAM domain, a region previously identified as being crucial for STIM1 function. So far, the role of the STIM1 EF-SAM domain has been uniquely associated with SOCE activation (Stathopoulos et al., 2006, 2008) whereas gain-of-function mutations in the EF-hand domain have only been associated with the constitutive activation of STIM1 and SOCE (Böhm et al., 2013; Lacruz and Feske, 2015; Noury et al., 2017). Here, we reveal a gain of function for the STIM1-E152K variant potentially caused by altered interactions with SERCA rather than enhanced EF-SAM oligomerization. This modification leads to deregulated  $\text{Ca}^{2+}$  homeostasis through its interaction with SERCA and trypsin autoactivation, thereby triggering cell death. SERCA has been previously shown to interact with STIM1 and has been determined to be a fundamental component of the store-operated  $\text{Ca}^{2+}$  influx complex (SOCIC) formed by channels and proteins regulating SOCE and store refilling (Jousset et al., 2007; López et al., 2008; Manjarrés et al., 2010; Vaca, 2010).

The enhancement of SERCA pump activity after store depletion explains the increase in  $[\text{Ca}^{2+}]_{\text{ER}}$  and  $\text{Ca}^{2+}$  release observed in STIM1-E152K-expressing cells. As proposed by López and colleagues (2008), STIM1 is already associated directly or indirectly with SERCA before store depletion under our experimental conditions. However, our study is the first to propose a SERCA pump conformational change when STIM1 is mutated in a specific locus. We propose that the conformational change of SERCA in the presence of STIM1-E152K under resting conditions is responsible for the enhancement of SERCA pump



activity and subsequently for the amplification of  $[Ca^{2+}]_{ER}$  and ER  $Ca^{2+}$  release. An E152K variant favors the cytoplasmic 'opened' state, which occurs prior to the conformational change after  $Ca^{2+}$  depletion. Regulation of  $Ca^{2+}$  pump function via a physical

interaction has been previously demonstrated for the plasma membrane  $Ca^{2+}$  ATPase (PMCA) (Ritchie et al., 2012).

It is now clearly established that the cell damage observed in pancreatitis originates from an abnormal increase in or maintained

level of  $[Ca^{2+}]_i$  (Petersen, 2009). Initial release of  $Ca^{2+}$  from both the ER and acidic pools in the apical region of pancreatic acinar cells is the critical starting point for the  $Ca^{2+}$ -dependent activation of pro-enzymes, such as trypsinogen. Expressing the STIM1-E152K variant in AR42J pancreatic cells clearly induces excessive  $Ca^{2+}$  release from the ER after cell stimulation that could be correlated with the cytotoxicity observed under these conditions, resulting from an increased basal trypsin activity along with decreased secretion of its trypsinogen precursor after cell stimulation. Regulation of cationic trypsinogen degradation and auto-activation along with trypsin inactivation are key protective mechanisms from pancreatic injury reported as being sensitive to  $Ca^{2+}$  (Szmola and Sahin-Tóth, 2007; Szabó et al., 2014).

In pancreatic acinar cells, the role of  $Ca^{2+}$  in zymogen granule secretion is well established (Messenger et al., 2014). The main role of ER  $Ca^{2+}$  release in the apical granular region of pancreatic acinar cells is to generate  $Ca^{2+}$  transients in local micro-domains to activate acinar fluid and enzyme secretion by exocytosis (Maruyama et al., 1993; Maruyama and Petersen, 1994; Petersen, 2015). Tightly regulated apical ER SERCA pump activity is therefore crucial for providing an optimal environment for controlled local  $Ca^{2+}$  signaling and regulated zymogen exocytosis. Excessive release of  $Ca^{2+}$  from the ER and subsequent perturbation in apical  $Ca^{2+}$  micro-domains have been linked to the major apical region structural and functional disorganization observed in pancreatitis, such as the appearance of endocytic vacuoles in which trypsinogen has been transformed to active trypsin and mitochondrial depolarization (Gerasimenko et al., 2009; Petersen, 2015). Taken together, we surmise that the expression of some gain-of-function *STIM1* variants that enhance ER  $Ca^{2+}$  release may promote acinar cell damage thereby contributing to the etiology of chronic pancreatitis.

In summary, we have provided a number of pieces of evidence to support the view that a *STIM1* variant, p.E152K, could act as a disease modifier by causing specific changes in  $Ca^{2+}$  homeostasis that in turn increase intracellular trypsin activation and cell death. This finding may prompt new lines of research into ICP as well as opening new avenues for future therapeutic studies into the development of drugs designed to modulate  $Ca^{2+}$  signaling, with a view to preventing, or at least delaying, the transition from acute pancreatitis to chronic pancreatitis (Wen et al., 2015). Moreover, the identification of the *STIM1* p.E152K variant together with three known disease-predisposing variants (in three different trypsin-dependent pathway genes) in the same patient provided an exceptionally illustrative example for the complex etiology of chronic pancreatitis. Finally, this study led to the identification of a previously undescribed change in SERCA properties in the presence of mutations in the *STIM1* EF-SAM domain, thereby generating new insights into the structure and function of *STIM1*.

## MATERIALS AND METHODS

### Reagents

Thapsigargin, cholecystokinin, carbachol, ATP, benzamidine, tBHQ, CCCP and digitonin were obtained from Sigma. Fura-2 BZiPAR and Protein G magnetic beads were from Invitrogen Thermo Fisher Scientific (Waltham, MA). LipoD293 was from Tebu-bio (Le Perray-en-Yvelines, France). D1ER was kindly provided by Nicolas Demareux (Department of Cell Physiology and Metabolism, Faculty of Medicine, University of Geneva, Geneva, Switzerland). Anti-PRSS1 antibody was obtained from R&D Systems (Minneapolis, MN), *STIM1* antibody from BD Transduction Laboratories (Franklin Lakes, NJ), anti-GAPDH antibody from Tebu-Bio, anti-SERCA antibody from Santa Cruz Biotechnology (Dallas, TX) and anti-sheep-IgG secondary antibody was from R&D Systems. The ER-targeted cameleon probe D1ER was kindly provided by Drs Amy Palmer

and Roger Tsien (University of California, San Diego, La Jolla, CA). ORAI1 construct, YFP *STIM1* and *STIM1* CFP were generous gifts from Drs Trevor Shuttleworth (Department of Pharmacology and Physiology, University of Rochester Medical Center, Rochester, NY), Anant B. Parekh (Department of Physiology, Anatomy and Genetics, University of Oxford, Oxford, UK) and Anjana Rao (Center for Autoimmunity and Inflammation, La Jolla Institute for Immunology, La Jolla, CA), respectively.

### Construction of *STIM1* cDNA expression vector and mutagenesis

RNA was extracted with Trizol (Invitrogen, Carlsbad, CA) from Colo-357 cells. The SuperScript<sup>®</sup> II Reverse Transcriptase, random hexamers (Qiagen, Courtaboeuf, France) and 2  $\mu$ g RNA were used to synthesize first strand cDNA. RT-PCR was performed using the Phusion<sup>®</sup> High-Fidelity DNA Polymerase (NEB, Evry, France) according to the manufacturer's protocol in a 50- $\mu$ l reaction mixture using forward primer 5'-ATGGATGTATGCGTCCGTCT-3' and reverse primer 5'-CTACTTCTTAAAGAGGCTTCT-3'. The PCR program comprised an initial denaturation at 98°C for 30 s, followed by 40 cycles denaturation at 98°C for 20 s, annealing at 62°C for 20 s and extension at 72°C for 90 s, with a final extension at 72°C for 5 min. After migration in a 1% agarose gel, the expected band (2058 bp) was purified using the MinElute PCR Purification Kit (Qiagen, Courtaboeuf, France). After adding the 3' A-overhangs to the PCR-purified product, the *STIM1* cDNA was cloned into the pcDNA3.1/V5-His TOPO TA vector (Invitrogen, Cergy-Pontoise, France). All *STIM1* variants were generated from the wild-type (WT) construct by site-directed mutagenesis using the QuikChange II XL Site-Directed Mutagenesis Kit (Stratagene, Massy, France). All resulting plasmids were checked by Sanger sequencing.

### Extraction of fibroblasts

Skin biopsies were washed in PBS, cut into small pieces and placed on 60 mm coated plates (Corning<sup>®</sup> CellBIND<sup>®</sup> Surface, Corning). Fibroblast expansion was made in DMEM completed with 10% FBS and 100 U/ml penicillin/streptomycin in a humidified incubator with 5%  $CO_2$  at 37°C. After the fibroblasts had colonized the plate, explants were removed, and fibroblasts expanded. At confluence, cells were trypsinized. Cells were used from passages 3 to 6, and placed on coverslips for image analysis. Consent was obtained from all individuals and the protocol was approved by the Ethical Board at the Brest University Hospital, in accordance with the Declaration of Helsinki.

### Cytosolic $Ca^{2+}$ measurements

Cells were plated on 18 mm glass cover slips. Changes in cytosolic  $Ca^{2+}$  concentration were measured with Fura-2 (Thermo Fisher Scientific). Cells were loaded with 4  $\mu$ M Fura-2/AM for 45 min in the dark at room temperature in a medium containing 135 mM NaCl, 5 mM KCl, 1 mM  $MgCl_2$ , 1.8 mM  $CaCl_2$ , 10 mM Hepes, 10 mM glucose, pH 7.4. The  $Ca^{2+}$ -free solution contained 1 mM EGTA instead of 1.8 mM  $CaCl_2$ . Cells were washed and equilibrated for 15 min in the same buffer to allow de-esterification of the dye. Ratiometric images of  $Ca^{2+}$  signals were obtained at room temperature using a microscope (IX71, Olympus) equipped with a monochromator illumination system (Polychrome V, TILL Photonics). Cells were illuminated alternately at 340 nm and 380 nm, and emission was collected every 3 s through a 415DCLP dichroic mirror at 435 nm by a 14-bit CCD camera (EXiBlue, Qimaging). Image acquisition and analysis were performed with the Metafluor 6.3 software (Universal Imaging, West Chester, PA). The excitation/emission ratio was calculated for each cell. For normalization, the formula  $(F-F_0)/F_0$ , was used, where F is the excitation/emission ratio of each value and  $F_0$  is the initial ratio. 'Speed of ER release' was calculated as the maximal  $dF/dt$  (increase in  $\Delta F/F_0$ /time) and 'Amplitude on ER release' was calculated as the maximal amplitude obtained from the  $\Delta F/F_0$  time curve.

### ER $Ca^{2+}$ measurements

HEK293T cells (ATCC) were transiently transfected using LipoD293 (tebu-bio) with 2  $\mu$ g cDNA encoding the D1ER construct 48 h before the experiments. Ratiometric images of  $Ca^{2+}$  signals were obtained

using a microscope (Axio Observer, Zeiss) equipped with a Lambda DG4 illumination system (Sutter Instrument Company, Novato, CA) as previously described (Philippe et al., 2015). *In situ* calibration of D1ER was performed in medium containing 10 mM NaCl, 135 mM KCl, 1 mM MgCl<sub>2</sub>, 20 mM sucrose, 20 mM Hepes, 0.01 mM digitonin, 0.01 mM ionomycin, 0.005 mM CCCP (pH 7.1 with NaOH). 5 mM EGTA and 5 mM EDTA were used to buffer free [Ca<sup>2+</sup>] below 100 μM, and 10 mM EDTA to buffer free [Ca<sup>2+</sup>] between 100 μM and 1 mM (Max Chelator Winmaxc version 2.51). To evaluate the resting ER Ca<sup>2+</sup> concentration, minimum and a maximum D1ER fluorescence values were measured at the end of each experiment. To quantify ER Ca<sup>2+</sup> refilling, the slope of the increase of FRET signal was determined by a linear fit. To measure Ca<sup>2+</sup> leak rates of the ER, passive ER depletion was induced by thapsigargin and the D1ER responses were fitted with a one-phase exponential decay function to extract the half-time (τ<sub>1/2</sub>).

For experiments with permeabilized HEK cells, cells were permeabilized by the addition of 60 μM digitonin (1 min) after ER Ca<sup>2+</sup> depletion by 15 μM tBHQ (15 min in Ca<sup>2+</sup>-free medium). ER Ca<sup>2+</sup> refilling was then measured by allowing them to recover in intracellular buffer before the addition of 100 nM CaCl<sub>2</sub> plus 2.5 μM CCCP (to block mitochondrial Ca<sup>2+</sup> uptake). To mimic cytosolic ionic composition in these permeabilizing experiments, HEK293T cells were washed with high K<sup>+</sup> intracellular buffer, containing 110 mM KCl, 10 mM NaCl, 0.5 mM K<sub>2</sub>HPO<sub>4</sub>, 5 mM succinate, 10 mM HEPES (pH 7.0 at 37°C), supplemented with 5 mM EDTA or 1 mM EGTA. 100 nM [Ca<sup>2+</sup>] was calculated using the Maxchelator program.

#### Assessment of SERCA conformational changes

FRET imaging experiments were performed using an epifluorescence inverted microscope (DMIRE-2, Leica) with a PlanApo 40× oil immersion objective. The excitation light source was a high-speed scanning polychromator with a Xe lamp (C7773, Hamamatsu Photonics). An emission filter wheel was controlled by a Lambda-10 device (Sutter Instruments). Images were acquired with an ORCA-FLASH 4.0 camera (C11440-22CU) and Aquacosmos 2.6 software was used to control all devices. Both camera and software were from Hamamatsu Photonics. ImageJ software was used for analyses.

Cells were plated in 35 mm ibidi μ-dishes, and transfected with Lipofectamine 2000. The SERCA2a conformation sensor was labeled with GFP in the N-terminus and tagRFP in the nucleotide domain. Transfections were performed using RG-SERCA and either empty vector, CFP-WT STIM1 or CFP-E152K-STIM1 (1 μg:0.5 μg DNA). Cells were perfused in a medium containing 135 mM NaCl, 5 mM KCl, 1 mM MgCl<sub>2</sub>, 1.8 mM CaCl<sub>2</sub>, 10 mM Hepes, 10 mM glucose, pH 7.4. The Ca<sup>2+</sup>-free solution contained 1 mM EGTA instead of 1.8 mM CaCl<sub>2</sub>. Cells were illuminated at 500 nm through an excitation filter (422/503/572 nm) and a triple-edge dichroic mirror (422/520/590 nm). FRET and donor emissions were alternately collected with emission filters 620/52 nm and 535/22 nm (denoted as center wavelength/bandwidth), respectively. A ratio of FRET image (donor excitation, acceptor emission) and donor image (GFP) (donor excitation, donor emission) was calculated, after subtracting background in both channels for its analysis. STIM1 expression was checked by excitation at 430 nm while emission was collected with emission filter 475/20 nm.

#### Western blotting

Cells were washed in ice-cold PBS and lysed with RIPA buffer containing protease inhibitor cocktail (Sigma-Aldrich) at 4°C for 30 min. Cell lysates were centrifuged at 16,000 g for 10 min at 4°C, and supernatants were collected. Cell lysates (100 μg) were loaded, separated in acrylamide SDS-PAGE gel (gradient 4–12%), and transferred to a PVDF membrane. For experiments designed to evaluate trypsin secretion, the conditioned medium was treated with trichloroacetic acid for protein precipitation and washed three times in acetone. Blots were incubated with anti-PRSS1 antibody (1:1000), anti-STIM1 antibody (1:1000) or anti-GAPDH antibody (1:2000) and probed with a peroxidase-conjugated anti-mouse-IgG antibody (1:2000) or anti-sheep-IgG secondary antibody (1:2000). An enhanced chemiluminescence system was used for visualization.

#### Immunoprecipitation

Anti-SERCA antibody was coupled to Protein G beads (GE Healthcare) by incubating 2.5 μg antibody with the beads (30 μl) for 2 h at 4°C. Cells from 100 mm plaques were washed in ice-cold PBS and treated with lysis buffer containing protease inhibitor cocktail at 4°C for 30 min. Cell lysates were centrifuged at 14,000 g for 15 min at 4°C, and supernatants were collected. Whole-cell lysates were added into the beads coupled to the antibody and incubated under gentle agitation for 2 h at 4°C. Precipitated proteins were eluted with SDS-sample buffer, incubated at 100°C for 10 min, centrifuged and the supernatants were loaded to perform the electrophoresis of the gels.

#### STIM1 oligomerization

1 μg of CFP-STIM1 constructs and 3 μg YFP-STIM1 constructs were co-transfected and cells were imaged 48 h after transfection. The oligomerization of STIM1 was followed by measuring the FRET signal between CFP- and YFP-STIM1. Cells were excited at 430 nm through a 455-nm dichroic mirror (455DRLP, Omega Optical), and emission was collected alternately at 480 and 535 nm (480AF30 and 535DF25, Omega Optical).

#### BZiPAR assay

Cells were incubated with 100 μM of the trypsin substrate BZiPAR (Thermo Fisher Scientific, Waltham, MA) for 120 min. Cells were excited at 494 nm for 150 ms, and fluorescence emission was collected at 535 nm. A T510lpxrt dichroic filter and an ET535/50 emission filter, both from Chroma Technology (Bellows Falls, VT) were used. Trypsin was added to confirm the increase in fluorescence signal when BZiPAR was present. The trypsin inhibitor benzamide (5 μg/ml) was used to check specific trypsin response. The fluorescence (excitation 494 nm, emission 535 nm) was measured from each cell to compare among conditions.

#### Cytotoxicity assay

Cell toxicity was measured using the CellTox™ Green Cytotoxicity Assay kit (Promega), and results were normalized to living cell numbers as evaluated with the CellTiter 96® Aqueous One Solution Cell Proliferation Assay Kit (Promega) following the manufacturer's instructions. Absorbance, which is proportional to living cell numbers, was measured at 490 nm. The cell cytotoxicity test is based on cellular membrane integrity using a cyanine dye with significant affinity for the DNA of dying cells. The dye properties are modified when fixed to DNA and fluorescence is enhanced. Emitted fluorescence (excitation, 512 nm, emission, 532 nm) is proportional to cell cytotoxicity and was measured for each experimental condition at different time points following the manufacturer's instructions. Cytotoxicity results were normalized using cell titration data.

#### Recombinant EF-SAM protein expression and purification

The T153I and E152K variants were separately introduced into pET-28a expression vectors (Merck Millipore) using the Quikchange protocol (Agilent, Inc.). The pET-28a vectors were transformed into BL21 DE3 CodonPlus *E. coli* cells by heat shock, and liquid Luria-Bertani cultures were grown at 37°C until the optical density (600 nm) reached 0.6. Protein expression was subsequently induced with 0.3 mM isopropyl β-D-thiogalactopyranoside and allowed to progress overnight. The hexahistidine (His6)-tagged proteins of interest were captured from *E. coli* cell lysate using Ni-nitriloacetic acid agarose resin (Qiagen) under denaturing conditions according to the manufacturer's guidelines. EF-SAM was refolded by dilution into 20 mM Tris-HCl, 150 mM NaCl, 5 mM CaCl<sub>2</sub>, pH 8. Subsequently, the His6-tags were cleaved by thrombin digestion and a final size exclusion chromatography purification step using a Superdex 200 10/300 GL column linked with an AKTA FPLC (GE Healthcare, Inc.) was performed to achieve a purity of >95%.

#### Far-UV-CD

Circular dichroism (CD) data were acquired on a Jasco J-815 CD spectrometer (Jasco, Inc.) collected in 1 nm increments (20 nm min<sup>-1</sup>) using a 0.1 cm path length cuvette, 8 s averaging time and 1 nm bandwidth at 20°C. Thermal melts were acquired by monitoring the change in the 225 nm CD signal as a function of temperature (i.e. 4–75°C) using 0.1 cm

cuvettes, 8 s averaging time, 1 nm bandwidth and 1°C min<sup>-1</sup> scan rate. Spectra were corrected for buffer contributions.

### SEC-MALS

MALS measurements were performed in-line with the size exclusion chromatography using a three angle (i.e. 45°, 90° and 135°) miniDawn light scattering instrument equipped with a 690 nm laser and an Optilab rEX differential refractometer (Wyatt Technologies, Inc.). Molecular mass was calculated using ASTRA software (Wyatt Technologies, Inc.) based on Zimm plot analysis and using a protein refractive index increment,  $dn/dc = 0.185 \text{ l g}^{-1}$ .

### Bioinformatics and modeling programs

Molecular modeling studies were performed using a Dell Precision 490 workstation running on Fedora 8 Linux with dual Xeon 3.06 GHz processors, 4 GB RAM, and a 250 GB hard drive. Schrödinger's Maestro 9.3 (Yang et al., 2006) belonging to the Schrödinger Suite 2012 was used as the graphical user interface for preparing the molecular structures. Maestro and Macromodel 9.9 (Schrödinger, LLC, New York, 2012) were used in preparation and minimization of the protein prior to docking studies. PyMol from DeLano Scientific and Maestro (DeLano Scientific, Palo Alto, CA, USA, 2002) were used for graphical presentation of the results.

### Preparation of the virtual protein structure

Prior to docking, the crystal structure of the protein (PDB ID: 2K60) (Stathopoulos et al., 2008), solved from nuclear magnetic resonance (NMR) data was retrieved from the Protein Data Bank (Berman et al., 2000). All water molecules were deleted and then Schrödinger's ProteinPrep (Schrödinger Suite 2012 Protein Preparation Wizard; Epik version 2.3; Impact version 5.8, Schrödinger, Prime version 3.1, Schrödinger) application was used with default settings to prepare and refine the protein, which included assigning bond order, addition of explicit hydrogens, creating zero-order bonds for metals and creating disulfide bonds. Energy minimization was performed to the point where heavy atoms converged to a 0.3 Å root-mean-square deviation (RMSD). The force field used here was OPLS 2005.

### Molecular dynamics

Molecular dynamics (MD) studies were performed on the STIM1 luminal and transmembrane portions of the WT and E152K mutant STIM1 protein structures. Schrödinger's Prime 3.1 was used to build the homology model of the luminal portion (2K60) and the transmembrane protein, with the final structures representing residues 58–201. The mutant structure was generated by converting the E152 residue into a lysine residue, and residues 202–236 were added to provide the transmembrane residues so that the structure could be placed in a simulated membrane. Variant E152K was introduced into the structure using Maestro and then both the mutated and non-mutated structures were energy minimized using NAMD in the presence of a 1-palmitoyl-2-oleoyl-sn-glycero-3-phosphocholine (POPC) membrane. POPC is a lipid bilayer membrane lipid present naturally in cell membranes. NAMD was developed by the Theoretical and Computational Biophysics Group at the Beckman Institute for Advanced Science and Technology at the University of Illinois at Urbana–Champaign. It is a parallel MD program designed for high-performance simulation of biological systems (Phillips et al., 2005). NAMD uses the molecular graphics program VMD (Visual Molecular Dynamics) for simulation setup and analysis (Humphrey et al., 1996).

Herein, the VMD software Version 1.6. Psfgen plugin was used initially to generate a Protein Structure File (psf) of the protein from its PDB format file. PsfGen involves using a prepared PDB file of the protein followed by reading the topology files and aligning the residues to match the PDB file to the topology files. The entire structure is then built and other fixes are performed to write a final psf of the protein that is used in the simulation.

The system is then neutralized with Na<sup>1+</sup> and Cl<sup>1-</sup> ions, with the addition of extra ions to have the system at 0.2 mol/l (*in vivo* concentration); finally, addition of TIP3P water, which uses the CHARMM force field, to the whole system generates a box of 205×205×205 Å. The protein was placed into the membrane using VMD. MD simulations on the mutated and non-mutated STIM1s were run for 35 ns and 45 ns respectively to see convergence. Final

frames were used for analysis. Structural alignments were performed with Dali (Holm and Sander, 1995) and DaliLite (Holm and Park, 2000), while sequence alignments were performed using CLUSTAL W (Larkin et al., 2007). Molecular images were rendered using PyMOL (Delano, 2002). Electrostatic potential was calculated and rendered in MOLMOL (Koradi et al., 1996). The 'closed' EF-SAM model was calculated with Modeller (Fiser and Šali, 2003) using the apo C-terminal CaM structure (PDB ID: 1F71) for the EF-hand domain, the NMR structure defined herein for the SAM domain and sequence alignments between CaM and EF-SAM performed with CLUSTAL W.

### Note on computational modeling of the E152K mutant

Molecular dynamics simulations pointed out that the converged structures for the WT and E152K variant proteins displayed superficial differences in appearance with regard to their partial charge surface distributions (Fig. S3A). Residue side chains could move freely but the underlying  $\alpha$ -helices remained similar (Fig. S3B) except for the N-terminal helix (red). However, there were distinct differences between the two modeled proteins around the residue 152 site (Fig. S3C). Whereas the WT STIM1 manifests hydrogen bonds between E152 and neighboring residues K156 and R155, and E152 remains just at or below the protein surface (Fig. S3C, left), the cationic K152 residue in the mutant STIM1 did not display ionic interactions and protruded out from the protein surface as did the K156 residue (Fig. S3C, right). In some conformations among the converged mutant STIM1 frames, the R155 residue was positioned below the surface with hydrogen bonding to the backbone, whereas in other conformations, R155 was sticking out towards the solvent between E151 and K152, providing an additional cationic side chain exposed to the environment. Local changes in surface electrostatics were consistent with these structural changes with mutant STIM1 displaying a strong cationic surface around the K152 site (blue, Fig. S3A, lower panel) whereas the WT E152 site is neutral to slightly anionic (red and white, Fig. S3A, upper panel). This difference in local charge linked with the surface accessibility of the K152 and K156 (and sometimes R155) would affect protein–protein interactions of the SAM domain.

### Statistical analyses

Sets of functional analytic data were compared using analysis of variance (one-way ANOVA with Tukey's post hoc test) or a unpaired two-tailed Student's *t*-test. \**P*<0.05; \*\**P*<0.001; \*\*\**P*<0.0005; \*\*\*\**P*<0.0001. Data shown are from at least four independent experiments.

### Acknowledgements

We thank Dr N. Demareux (Geneva, Switzerland) for generously providing the D1ER plasmid, Drs R. Y. Tsieng (La Jolla, CA) and A. Palmer (La Jolla, CA) for providing the cameleon. We are grateful to M. Henry (Brest, France), A. Youinou (Brest, France) and L. Leroi (Brest, France) for technical support. We also thank C. Castelbou (Geneva, Switzerland) for technical assistance.

### Competing interests

The authors declare no competing or financial interests.

### Author contributions

Conceptualization: M.B., T.C., O.M.; Methodology: M.B., N.L., P.B.S., M.I., O.M.; Validation: M.F., J.L., M.I., W.B., O.M.; Formal analysis: M.B.; Investigation: M.B., R.P., F.A., P.B., E.M., S.M., P.D., C.L.M., F.C., N.L., M.F., B.D., P.B.S., M.I., W.B., W.G., J.-M.C.; Resources: J.L., C.F., O.M.; Writing - original draft: M.B., O.M.; Writing - review & editing: M.B., J.L., P.B.S., W.B., J.-M.C., T.C., O.M.; Visualization: M.B.; Supervision: J.L., O.M.; Project administration: O.M.; Funding acquisition: C.F., O.M.

### Funding

M.B. was supported by the Association de Transfusion Sanguine et de Biogénétique Gaetan Saleun, the Ministerio de Economía y Competitividad (Spanish Ministry of Economy and Competitiveness), reference BFU2015-69874-R and the Castilla-La Mancha Government, reference II-2018\_11. R.P. and O.M. were supported by the French association Vaincre La Mucoviscidose and the Association de Transfusion Sanguine et de Biogénétique Gaetan Saleun. F.A. was supported by a post-doctoral

grant from Aviesan (ITMO IHP). M.F. was supported by the Schweizerischer Nationalfonds zur Förderung der Wissenschaftlichen Forschung (Swiss National Foundation) grant # 310030-141113, the Association des Pancréatites Chroniques Hérititaires and the Institut National de la Santé et de la Recherche Médicale (INSERM), France. This work was supported by Canadian Institutes of Health Research (CIHR), Heart and Stroke Foundation of Canada (HSFC) and NSERC operating grants to M.I. and a Natural Sciences and Engineering Research Council of Canada (NSERC) operating grant to P.S.

### Supplementary information

Supplementary information available online at  
<https://jcs.biologists.org/lookup/doi/10.1242/jcs.244012.supplemental>

### Peer review history

The peer review history is available online at  
<https://jcs.biologists.org/lookup/doi/10.1242/jcs.244012.reviewer-comments.pdf>

### References

- Berman, H. M., Westbrook, J., Feng, Z., Gilliland, G., Bhat, T. N., Weissig, H., Shindyalov, I. N. and Bourne, P. E. (2000). The protein data bank. *Nucleic Acids Res.* **28**, 235-242. doi:10.1093/nar/28.1.235
- Böhm, J., Chevessier, F., Maues De Paula, A., Koch, C., Attarian, S., Feger, C., Hantäi, D., Laforêt, P., Ghorab, K., Vallat, J.-M. et al. (2013). Constitutive activation of the calcium sensor STIM1 causes tubular-aggregate myopathy. *Am. J. Hum. Genet.* **92**, 271-278. doi:10.1016/j.ajhg.2012.12.007
- Delano, W. L. (2002). *The PyMOL Molecular Graphics System*. San Carlos, CA: DeLano Scientific LLC.
- Fiser, A. and Šali, A. (2003). Modeller: generation and refinement of homology-based protein structure models. *Methods Enzymol.* **374**, 461-491. doi:10.1016/S0076-6879(03)74020-8
- Gerasimenko, J. V., Lur, G., Sherwood, M. W., Ebisui, E., Tepikin, A. V., Mikoshiba, K., Gerasimenko, O. V. and Petersen, O. H. (2009). Pancreatic protease activation by alcohol metabolite depends on Ca<sup>2+</sup> release via acid store IP<sub>3</sub> receptors. *Proc. Natl. Acad. Sci. USA* **106**, 10758-10763. doi:10.1073/pnas.0904818106
- Gerasimenko, J. V., Gryshchenko, O., Ferdek, P. E., Stapleton, E., Hébert, T. O. G., Bychkova, S., Peng, S., Begg, M., Gerasimenko, O. V. and Petersen, O. H. (2013). Ca<sup>2+</sup> release-activated Ca<sup>2+</sup> channel blockade as a potential tool in antipancreatitis therapy. *Proc. Natl. Acad. Sci. USA* **110**, 13186-13191. doi:10.1073/pnas.1300910110
- Gerasimenko, J. V., Gerasimenko, O. V. and Petersen, O. H. (2014). The role of Ca<sup>2+</sup> in the pathophysiology of pancreatitis. *J. Physiol.* **592**, 269-280. doi:10.1111/jphysiol.2013.261784
- Harris, E., Burki, U., Marini-Bettolo, C., Neri, M., Scotton, C., Hudson, J., Bertoli, M., Evangelista, T., Vroiling, B., Polvikoski, T. et al. (2017). Complex phenotypes associated with STIM1 mutations in both coiled coil and EF-hand domains. *Neuromuscul. Disord.* **NMD 27**, 861-872. doi:10.1016/j.nmd.2017.05.002
- Hedberg, C., Niceta, M., Fattori, F., Lindvall, B., Ciolfi, A., D'Amico, A., Tasca, G., Petrin, S., Tulinius, M., Tartaglia, M. et al. (2014). Childhood onset tubular aggregate myopathy associated with de novo STIM1 mutations. *J. Neurol.* **261**, 870-876. doi:10.1007/s00415-014-7287-x
- Holm, L. and Park, J. (2000). DALI: a web server for protein structure comparison. *Bioinformatics* **16**, 566-567. doi:10.1093/bioinformatics/16.6.566
- Holm, L. and Sander, C. (1995). DALI: a network tool for protein structure comparison. *Trends Biochem. Sci.* **20**, 478-480. doi:10.1016/S0968-0004(00)89105-7
- Hou, Z., Hu, Z., Blackwell, D. J., Miller, T. D., Thomas, D. D. and Robia, S. L. (2012). 2-Color calcium pump reveals closure of the cytoplasmic headpiece with calcium binding. *PLoS ONE* **7**, e40369. doi:10.1371/journal.pone.0040369
- Humphrey, W., Dalke, A. and Schulten, K. (1996). VMD: visual molecular dynamics. *J. Mol. Graph.* **14**, 33-38, 27-38. doi:10.1016/0263-7855(96)00018-5
- Jousset, H., Frieden, M. and Demaurex, N. (2007). STIM1 knockdown reveals that store-operated Ca<sup>2+</sup> channels located close to sarco/endoplasmic Ca<sup>2+</sup> ATPases (SERCA) pumps silently refill the endoplasmic reticulum. *J. Biol. Chem.* **282**, 11456-11464. doi:10.1074/jbc.M609551200
- Kereszturi, E. and Sahin-Tóth, M. (2009). Intracellular autoactivation of human cationic trypsinogen mutants causes reduced trypsinogen secretion and acinar cell death. *J. Biol. Chem.* **284**, 33392-33399. doi:10.1074/jbc.M109.056812
- Koradi, R., Billeter, M. and Wüthrich, K. (1996). MOLMOL: a program for display and analysis of macromolecular structures. *J. Mol. Graph.* **14**, 51-55, 29-32. doi:10.1016/0263-7855(96)00009-4
- Krüger, B., Albrecht, E. and Lerch, M. M. (2000). The role of intracellular calcium signaling in premature protease activation and the onset of pancreatitis. *Am. J. Pathol.* **157**, 43-50. doi:10.1016/S0002-9440(10)64515-4
- Lacruz, R. S. and Feske, S. (2015). Diseases caused by mutations in ORAI1 and STIM1. *Ann. N. Y. Acad. Sci.* **1356**, 45-79. doi:10.1111/nyas.12938
- Larkin, M. A., Blackshields, G., Brown, N. P., Chenna, R., McGettigan, P. A., McWilliam, H., Valentin, F., Wallace, I. M., Wilm, A., Lopez, R. et al. (2007). Clustal W and Clustal X version 2.0. *Bioinformatics* **23**, 2947-2948. doi:10.1093/bioinformatics/btm404
- Liao, Y., Erxleben, C., Abramowitz, J., Flockerzi, V., Zhu, M. X., Armstrong, D. L. and Birnbaumer, L. (2008). Functional interactions among Orai1, TRPCs, and STIM1 suggest a STIM-regulated heteromeric Orai/TRPC model for SOCE/Icrac channels. *Proc. Natl. Acad. Sci. USA* **105**, 2895-2900. doi:10.1073/pnas.0712288105
- Liou, J., Kim, M. L., Heo, W. D., Jones, J. T., Myers, J. W., Ferrell, J. E. and Meyer, T. (2005). STIM is a Ca<sup>2+</sup> sensor essential for Ca<sup>2+</sup>-store-depletion-triggered Ca<sup>2+</sup> influx. *Curr. Biol.* **15**, 1235-1241. doi:10.1016/j.cub.2005.05.055
- López, J. J., Jardín, I., Bobe, R., Pariente, J. A., Enouf, J., Salido, G. M. and Rosado, J. A. (2008). STIM1 regulates acidic Ca<sup>2+</sup> store refilling by interaction with SERCA3 in human platelets. *Biochem. Pharmacol.* **75**, 2157-2164. doi:10.1016/j.bcp.2008.03.010
- Lur, G., Sherwood, M. W., Ebisui, E., Haynes, L., Feske, S., Sutton, R., Burgoyne, R. D., Mikoshiba, K., Petersen, O. H. and Tepikin, A. V. (2011). InsP<sub>3</sub> receptors and Orai channels in pancreatic acinar cells: co-localization and its consequences. *Biochem. J.* **436**, 231-239. doi:10.1042/BJ20110083
- Masson, E., Zou, W.-B., Ruffert, C., Holste, V., Michl, P., Mössner, J., Ewers, M., Laumen, H., Wu, H., Zhou, D.-Z. et al. (2019). Genetic analysis of the STIM1 gene in chronic pancreatitis. *bioRxiv*, 691899. doi:10.1101/691899
- Manjarrés, I. M., Rodríguez-García, A., Alonso, M. T. and García-Sancho, J. (2010). The sarco/endoplasmic reticulum Ca<sup>2+</sup> ATPase (SERCA) is the third element in capacitative calcium entry. *Cell Calcium* **47**, 412-418. doi:10.1016/j.ceca.2010.03.001
- Maruyama, Y. and Petersen, O. H. (1994). Delay in granular fusion evoked by repetitive cytosolic Ca<sup>2+</sup> spikes in mouse pancreatic acinar cells. *Cell Calcium* **16**, 419-430. doi:10.1016/0143-4160(94)90035-3
- Maruyama, Y., Inooka, G., Li, Y. X., Miyashita, Y. and Kasai, H. (1993). Agonist-induced localized Ca<sup>2+</sup> spikes directly triggering exocytotic secretion in exocrine pancreas. *EMBO J.* **12**, 3017-3022. doi:10.1002/j.1460-2075.1993.tb05970.x
- Masamune, A., Kotani, H., Sörgel, F. L., Chen, J.-M., Hamada, S., Sakaguchi, R., Masson, E., Nakano, E., Kakuta, Y., Niihori, T. et al. (2020). Variants that affect function of calcium channel TRPV6 are associated with early-onset chronic pancreatitis: TRPV6 and pancreatitis. *Gastroenterology* **158**, 1626-1641. doi:10.1053/j.gastro.2020.01.005
- Messenger, S. W., Falkowski, M. A. and Groblewski, G. E. (2014). Ca<sup>2+</sup>-regulated secretory granule exocytosis in pancreatic and parotid acinar cells. *Cell Calcium* **55**, 369-375. doi:10.1016/j.ceca.2014.03.003
- Misceo, D., Holmgren, A., Louch, W. E., Holme, P. A., Mizobuchi, M., Morales, R. J., De Paula, A. M., Stray-Pedersen, A., Lyle, R., Dalhus, B. et al. (2014). A dominant STIM1 mutation causes Stormorken syndrome. *Hum. Mutat.* **35**, 556-564. doi:10.1002/humu.22544
- Morin, G., Bruechle, N. O., Singh, A. R., Knopp, C., Jedraszak, G., Elbracht, M., Brémond-Gignac, D., Hartmann, K., Sevestre, H., Deutz, P. et al. (2014). Gain-of-function mutation in STIM1 (P.R304W) is associated with Stormorken syndrome. *Hum. Mutat.* **35**, 1221-1232. doi:10.1002/humu.22621
- Nesin, V., Wiley, G., Kousi, M., Ong, E.-C., Lehmann, T., Nicholl, D. J., Suri, M., Shahrzaila, N., Katsanis, N., Gaffney, P. M. et al. (2014). Activating mutations in STIM1 and ORAI1 cause overlapping syndromes of tubular myopathy and congenital miosis. *Proc. Natl. Acad. Sci. USA* **111**, 4197-4202. doi:10.1073/pnas.1312520111
- Noury, J.-B., Böhm, J., Peche, G. A., Guyant-Marechal, L., Bedat-Millet, A.-L., Chiche, L., Carlier, R.-Y., Malfatti, E., Romero, N. B. and Stojkovic, T. (2017). Tubular aggregate myopathy with features of Stormorken disease due to a new STIM1 mutation. *Neuromuscul. Disord.* **27**, 78-82. doi:10.1016/j.nmd.2016.10.006
- Nwokonko, R. M., Cai, X., Loktionova, N. A., Wang, Y., Zhou, Y. and Gill, D. L. (2017). The STIM-orai pathway: conformational coupling between STIM and Orai in the activation of store-operated Ca<sup>2+</sup> entry. *Adv. Exp. Med. Biol.* **993**, 83-98. doi:10.1007/978-3-319-57732-6\_5
- Pallikkuth, S., Blackwell, D. J., Hu, Z., Hou, Z., Zieman, D. T., Svensson, B., Thomas, D. D. and Robia, S. L. (2013). Phosphorylated phospholamban stabilizes a compact conformation of the cardiac calcium-ATPase. *Biophys. J.* **105**, 1812-1821. doi:10.1016/j.bpj.2013.08.045
- Palmer, A. E., Jin, C., Reed, J. C. and Tsien, R. Y. (2004). Bcl-2-mediated alterations in endoplasmic reticulum Ca<sup>2+</sup> analyzed with an improved genetically encoded fluorescent sensor. *Proc. Natl. Acad. Sci. USA* **101**, 17404-17409. doi:10.1073/pnas.0408030101
- Park, C. Y., Hoover, P. J., Mullins, F. M., Bachhawat, P., Covington, E. D., Raunser, S., Walz, T., Garcia, K. C., Dolmetsch, R. E. and Lewis, R. S. (2009). STIM1 clusters and activates CRAC channels via direct binding of a cytosolic domain to Orai1. *Cell* **136**, 876-890. doi:10.1016/j.cell.2009.02.014
- Parry, D. A., Holmes, T. D., Gamper, N., El-Sayed, W., Hettiarachchi, N. T., Ahmed, M., Cook, G. P., Logan, C. V., Johnson, C. A., Joss, S. et al. (2016). A homozygous STIM1 mutation impairs store-operated calcium entry and natural killer cell effector function without clinical immunodeficiency. *J. Allergy Clin. Immunol.* **137**, 955-957.e8. doi:10.1016/j.jaci.2015.08.051
- Petersen, O. H. (2009). Ca<sup>2+</sup> signaling in pancreatic acinar cells: physiology and pathophysiology. *Braz. J. Med. Biol. Res. Rev. Bras. Pesqui. Medicas E Biol.* **42**, 9-16. doi:10.1590/S0100-879X2009000100003

- Petersen, O. H. (2015).  $Ca^{2+}$  signalling in the endoplasmic reticulum/secretory granule microdomain. *Cell Calcium* **58**, 397-404. doi:10.1016/j.ceca.2015.01.006
- Philippe, R., Antigny, F., Buscaglia, P., Norez, C., Becq, F., Frieden, M. and Mignen, O. (2015). SERCA and PMCA pumps contribute to the deregulation of  $Ca^{2+}$  homeostasis in human CF epithelial cells. *Biochim. Biophys. Acta* **1853**, 892-903. doi:10.1016/j.bbamcr.2015.01.010
- Phillips, J. C., Braun, R., Wang, W., Gumbart, J., Tajkhorshid, E., Villa, E., Chipot, C., Skeel, R. D., Kalé, L. and Schulten, K. (2005). Scalable molecular dynamics with NAMD. *J. Comput. Chem.* **26**, 1781-1802. doi:10.1002/jcc.20289
- Picard, C., McCarl, C.-A., Papolos, A., Khalil, S., Lüthy, K., Hivroz, C., LeDeist, F., Rieux-Laucat, F., Rechavi, G., Rao, A. et al. (2009). STIM1 mutation associated with a syndrome of immunodeficiency and autoimmunity. *N. Engl. J. Med.* **360**, 1971-1980. doi:10.1056/NEJMoa0900082
- Raraty, M., Ward, J., Erdemli, G., Vaillant, C., Neoptolemos, J. P., Sutton, R. and Petersen, O. H. (2000). Calcium-dependent enzyme activation and vacuole formation in the apical granular region of pancreatic acinar cells. *Proc. Natl. Acad. Sci. USA* **97**, 13126-13131. doi:10.1073/pnas.97.24.13126
- Ritchie, M. F., Samakai, E. and Soboloff, J. (2012). STIM1 is required for attenuation of PMCA-mediated  $Ca^{2+}$  clearance during T-cell activation. *EMBO J.* **31**, 1123-1133. doi:10.1038/emboj.2011.495
- Roos, J., DiGregorio, P. J., Yeromin, A. V., Ohlsen, K., Lioudyno, M., Zhang, S., Safrina, O., Kozak, J. A., Wagner, S. L., Cahalan, M. D. et al. (2005). STIM1, an essential and conserved component of store-operated  $Ca^{2+}$  channel function. *J. Cell Biol.* **169**, 435-445. doi:10.1083/jcb.200502019
- Sampieri, A., Zepeda, A., Asanov, A. and Vaca, L. (2009). Visualizing the store-operated channel complex assembly in real time: identification of SERCA2 as a new member. *Cell Calcium* **45**, 439-446. doi:10.1016/j.ceca.2009.02.010
- Satoh, K., Matsu-Ura, T., Enomoto, M., Nakamura, H., Michikawa, T. and Mikoshiba, K. (2011). Highly cooperative dependence of sarco/endoplasmic reticulum calcium ATPase (SERCA) 2a pump activity on cytosolic calcium in living cells. *J. Biol. Chem.* **286**, 20591-20599. doi:10.1074/jbc.M110.204685
- Shen, W.-W., Frieden, M. and Demaurex, N. (2011). Local cytosolic  $Ca^{2+}$  elevations are required for stromal interaction molecule 1 (STIM1) deoligomerization and termination of store-operated  $Ca^{2+}$  entry. *J. Biol. Chem.* **286**, 36448-36459. doi:10.1074/jbc.M111.269415
- Sofia, V. M., Da Sacco, L., Surace, C., Tomaiuolo, A. C., Genovese, S., Grotta, S., Gnazzo, M., Ciocca, L., Petrocchi, S., Alghisi, F. et al. (2016). Extensive molecular analysis suggested the strong genetic heterogeneity of idiopathic chronic pancreatitis. *Mol. Med.* **22**, 300-309. doi:10.2119/molmed.2016.00010
- Son, A., Ahuja, M., Schwartz, D. M., Varga, A., Swaim, W., Kang, N., Maleth, J., Shin, D. M. and Muallem, S. (2019).  $Ca^{2+}$  influx channel inhibitor SARAF protects mice from acute pancreatitis. *Gastroenterology* **157**, 1660-1672.e2. doi:10.1053/j.gastro.2019.08.042
- Stathopoulos, P. B., Li, G.-Y., Plevin, M. J., Ames, J. B. and Ikura, M. (2006). Stored  $Ca^{2+}$  depletion-induced oligomerization of stromal interaction molecule 1 (STIM1) via the EF-SAM region: an initiation mechanism for capacitive  $Ca^{2+}$  entry. *J. Biol. Chem.* **281**, 35855-35862. doi:10.1074/jbc.M608247200
- Stathopoulos, P. B., Zheng, L., Li, G.-Y., Plevin, M. J. and Ikura, M. (2008). Structural and mechanistic insights into STIM1-mediated initiation of store-operated calcium entry. *Cell* **135**, 110-122. doi:10.1016/j.cell.2008.08.006
- Szabó, A., Radisky, E. S. and Sahin-Tóth, M. (2014). Zymogen activation confers thermodynamic stability on a key peptide bond and protects human cationic trypsin from degradation. *J. Biol. Chem.* **289**, 4753-4761. doi:10.1074/jbc.M113.538884
- Szmola, R. and Sahin-Tóth, M. (2007). Chymotrypsin C (caldecrin) promotes degradation of human cationic trypsin: identity with Rinderknecht's enzyme Y. *Proc. Natl. Acad. Sci. USA* **104**, 11227-11232. doi:10.1073/pnas.0703714104
- Vaca, L. (2010). SOCIC: the store-operated calcium influx complex. *Cell Calcium* **47**, 199-209. doi:10.1016/j.ceca.2010.01.002
- Vaeth, M., Maus, M., Klein-Hessling, S., Freinkman, E., Yang, J., Eckstein, M., Cameron, S., Turvey, S. E., Serfling, E., Berberich-Siebelt, F. et al. (2017). Store-operated  $Ca^{2+}$  entry controls clonal expansion of T cells through metabolic reprogramming. *Immunity* **47**, 664-679.e6. doi:10.1016/j.immuni.2017.09.003
- Waldron, R. T., Chen, Y., Pham, H., Go, A., Su, H.-Y., Hu, C., Wen, L., Husain, S. Z., Sugar, C. A., Roos, J. et al. (2019). The Orai  $Ca^{2+}$  channel inhibitor CM4620 targets both parenchymal and immune cells to reduce inflammation in experimental acute pancreatitis. *J. Physiol.* **597**, 3085-3105. doi:10.1113/JP277856
- Wen, L., Voronina, S., Javed, M. A., Awais, M., Szatmary, P., Latawiec, D., Chvanov, M., Collier, D., Huang, W., Barrett, J. et al. (2015). Inhibitors of ORAI1 prevent cytosolic calcium-associated injury of human pancreatic acinar cells and acute pancreatitis in 3 mouse models. *Gastroenterology* **149**, 481-492.e7. doi:10.1053/j.gastro.2015.04.015
- Wu, M. M., Buchanan, J. A., Luik, R. M. and Lewis, R. S. (2006).  $Ca^{2+}$  store depletion causes STIM1 to accumulate in ER regions closely associated with the plasma membrane. *J. Cell Biol.* **174**, 803-813. doi:10.1083/jcb.200604014
- Yang, X.-X., Hu, Z.-P., Chan, S. Y. and Zhou, S.-F. (2006). Monitoring drug-protein interaction. *Clin. Chim. Acta* **365**, 9-29. doi:10.1016/j.cca.2005.08.021
- Yuan, J. P., Kim, M. S., Zeng, W., Shin, D. M., Huang, G., Worley, P. F. and Muallem, S. (2009). TRPC channels as STIM1-regulated SOCs. *Channels Austin Tex* **3**, 221-225. doi:10.4161/chan.3.4.9198
- Zhu, Z.-D., Yu, T., Liu, H.-J., Jin, J. and He, J. (2018). SOCE induced calcium overload regulates autophagy in acute pancreatitis via calcineurin activation. *Cell Death Dis.* **9**, 50. doi:10.1038/s41419-017-0073-9
- Zou, W.-B., Tang, X.-Y., Zhou, D.-Z., Qian, Y.-Y., Hu, L.-H., Yu, F.-F., Yu, D., Wu, H., Deng, S.-J., Lin, J.-H. et al. (2018). SPINK1, PRSS1, CTSC, and CFTR genotypes influence disease onset and clinical outcomes in chronic pancreatitis. *Clin. Transl. Gastroenterol.* **9**, 204. doi:10.1038/s41424-018-0069-5

**Table S1.** Rate and amplitude ( $\Delta F/F$  % respect to WT) of calcium ER release and SOCE values of all 37 STIM variants identified in this study normalized to STIM1 values

Variant	ER release		SOCE	
	Rate	Amplitude	Rate	Amplitude
Empty vector	0.93	1.05	0.56	0.79
p.Ala31Pro	1.01	1.06	1.00	1.07
p.Ser36Leu	1.02	0.97	1.08	0.97
p.Ala38Pro	1.34	1.21	1.01	1.05
p.Ala38Val	0.98	0.98	0.90	0.91
p.Glu136Asp	0.89	0.94	0.95	0.95
p.Glu152Lys	1.68	1.57	1.05	0.92
p.Thr153Ile	1.14	1.02	1.00	0.92
p.Gln158Glu	0.96	0.94	0.96	0.98
p.Thr177Ile	0.90	1.00	0.92	0.97
p.Glu249Asp	1.00	0.99	1.06	1.07
p.Glu276Gln	1.02	0.98	1.01	1.00
p.Ser337Phe	0.90	1.10	0.85	0.98
p.Thr411Ala	0.88	0.89	0.82	0.90
p.Arg500Trp	1.14	1.12	0.95	1.03
p.Arg500Gln	1.10	1.04	1.01	1.00
p.Arg502His	1.22	1.11	0.94	0.95
p.Thr504Met	1.16	1.11	1.01	1.00
p.Ser521Leu	1.10	1.01	1.30	1.17
p.Ser524Phe	0.88	0.90	1.65	1.13
p.Ser528Asn	1.16	1.03	1.07	1.02
p.Arg530His	1.02	1.01	1.10	1.08
p.Arg532His	0.91	0.99	0.89	0.98
p.Ala534Asp	1.07	1.09	0.95	0.99
p.Pro538Ser	1.10	1.14	1.72	1.38
p.Gln539Ter	1.01	1.04	0.83	0.88

p.Arg542Cys	1.03	1.02	0.85	0.91
p.Glu546Lys	1.11	1.09	1.68	1.43
p.Ser556Arg	0.90	0.95	0.76	0.84
p.Arg558Gln	0.83	0.92	0.88	0.89
p.Glu561Lys	1.02	1.03	1.06	1.05
p.Pro601Ser	0.92	0.94	0.88	0.87
p.Ala603Val	0.95	0.94	0.80	0.85
p.Arg615Cys	1.16	1.03	1.00	1.05
p.Arg643His	1.01	1.06	1.01	1.04
p.Ala654Thr	0.95	1.05	1.05	1.08
p.Arg671Gln	1.22	1.10	1.03	1.01
p.Lys685Ter	1.14	1.05	0.97	0.95

All data were normalized against the wild-type values, which were set to 1. Values showing a statistically significant difference from that of the wild-type are highlighted in blue.

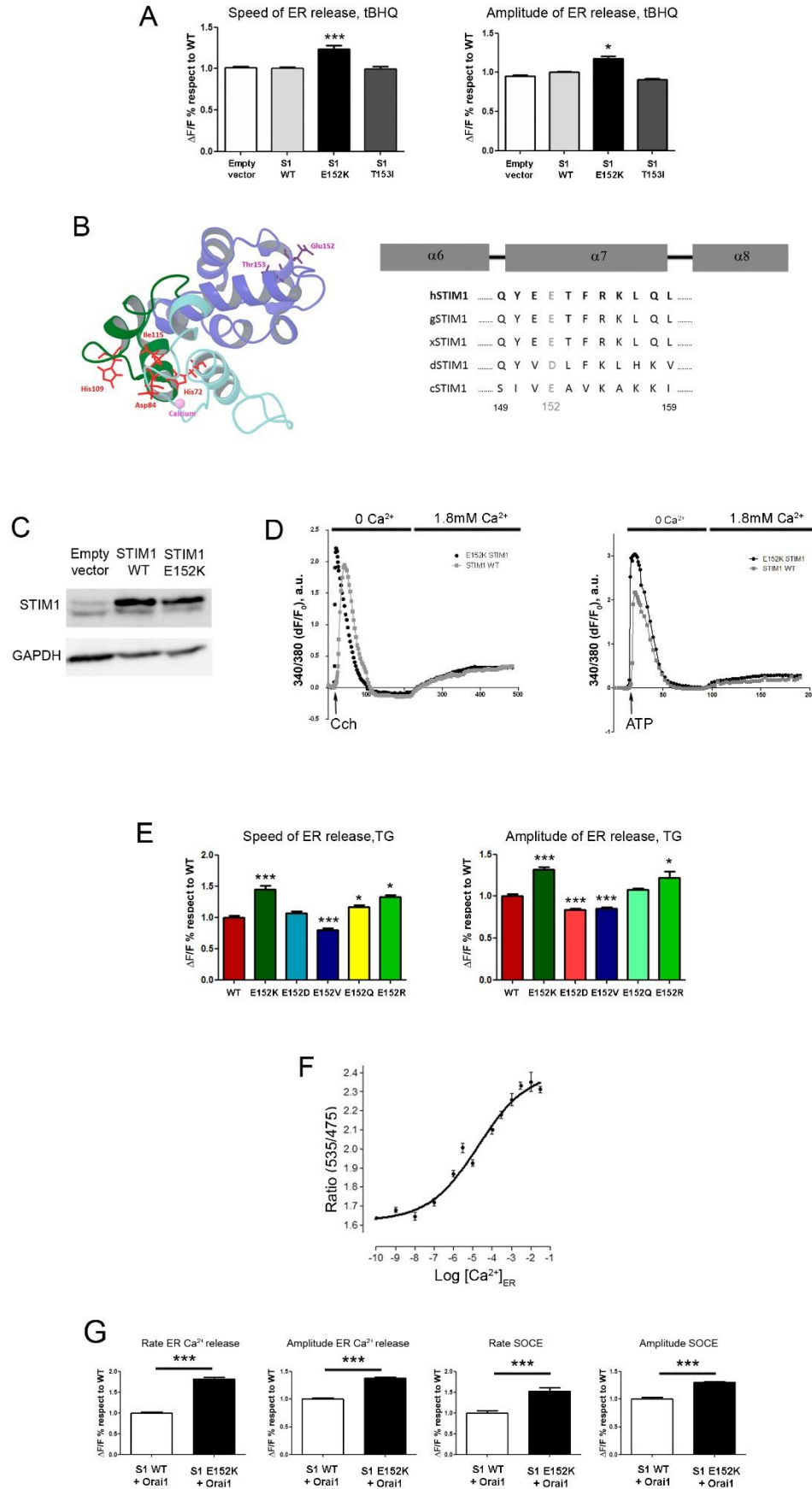


**Fig. S1. (A)**, Differences in the rate (left) and amplitude (right) of ER Ca<sup>2+</sup> release after cell stimulation by 15 μM tBHQ treatment in the absence of extracellular Ca<sup>2+</sup>. n = 838 (empty vector), 735 (WT), 740 (E152K), 693 (T153I). **(B)**, Secondary structure components of EF-hand (green) and SAM (purple) domains with variants identified in our study together with previously identified variants. The structural topology includes α1 (residues 64–73), β1 (82–83), α2 (89–97), α3 (102–108), β2 (115–116), α4 (117–126), α5 (128–131), α6 (134–145), α7 (150–157), α8 (161–168), α9 (171–174), α10 (183–199). α helices (ten in total) are represented by cylinders whereas β strands (two in total, making up one sheet) are depicted by arrowheads. Sequence alignments of the α7 helix from the EF-SAM domain within different species: hSTIM1, *Homo sapiens*; gSTIM1, *Gallus gallus*; xSTIM1, *Xenopus laevis*; dSTIM1, *Drosophila melanogaster*; cSTIM1, *Caenorhabditis elegans*. **(C)**, STIM1 expression in HEK293T cells as revealed by Western blot for WT, E152K STIM1 or an empty vector. GAPDH was used as a loading control. **(D)**, Representative traces of CCh (left) and ATP (right)-evoked Ca<sup>2+</sup> transients in Fura-2-loaded HEK293T cells expressing WT STIM1 or STIM1 E152K. **(E)**, Histograms representing rate of Ca<sup>2+</sup> ER release (left) and Ca<sup>2+</sup> amplitude (right) after TG treatment in HEK293T cells expressing the alternative STIM1 residue 152 variants. **(F)** *In situ* calibration of the D1ER probe in HEK cells. **(G)**, Histograms representing rate and amplitude of Ca<sup>2+</sup> ER release (left panels) and rate and amplitude of SOCE entry (right panels) after TG treatment in HEK293T cells double-transfected with WT STIM1/Orai1 or STIM1-E152K/Orai1.

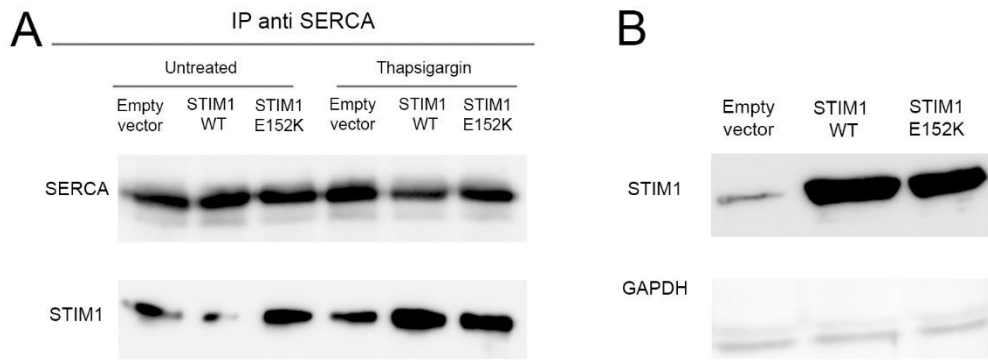


**Figure S2.** (A), 100mm plaques of HEK293 cells transfected with WT STIM1, E152K STIM1 or empty vector were left untreated or treated with 2  $\mu$ M TG in 1.8 mM Ca<sup>2+</sup> solution for 10 min and were subjected to immunoprecipitation with anti-SERCA antibody. Eluted fractions after immunoprecipitation (IP) and lysates were analyzed by SDS-PAGE and Western blot using anti-SERCA- and anti-STIM1-specific antibodies. (B), Western blot image of samples run in parallel to check the equal overexpression of WT STIM1 and STIM1-E152K regarding this immunoprecipitation experiment.

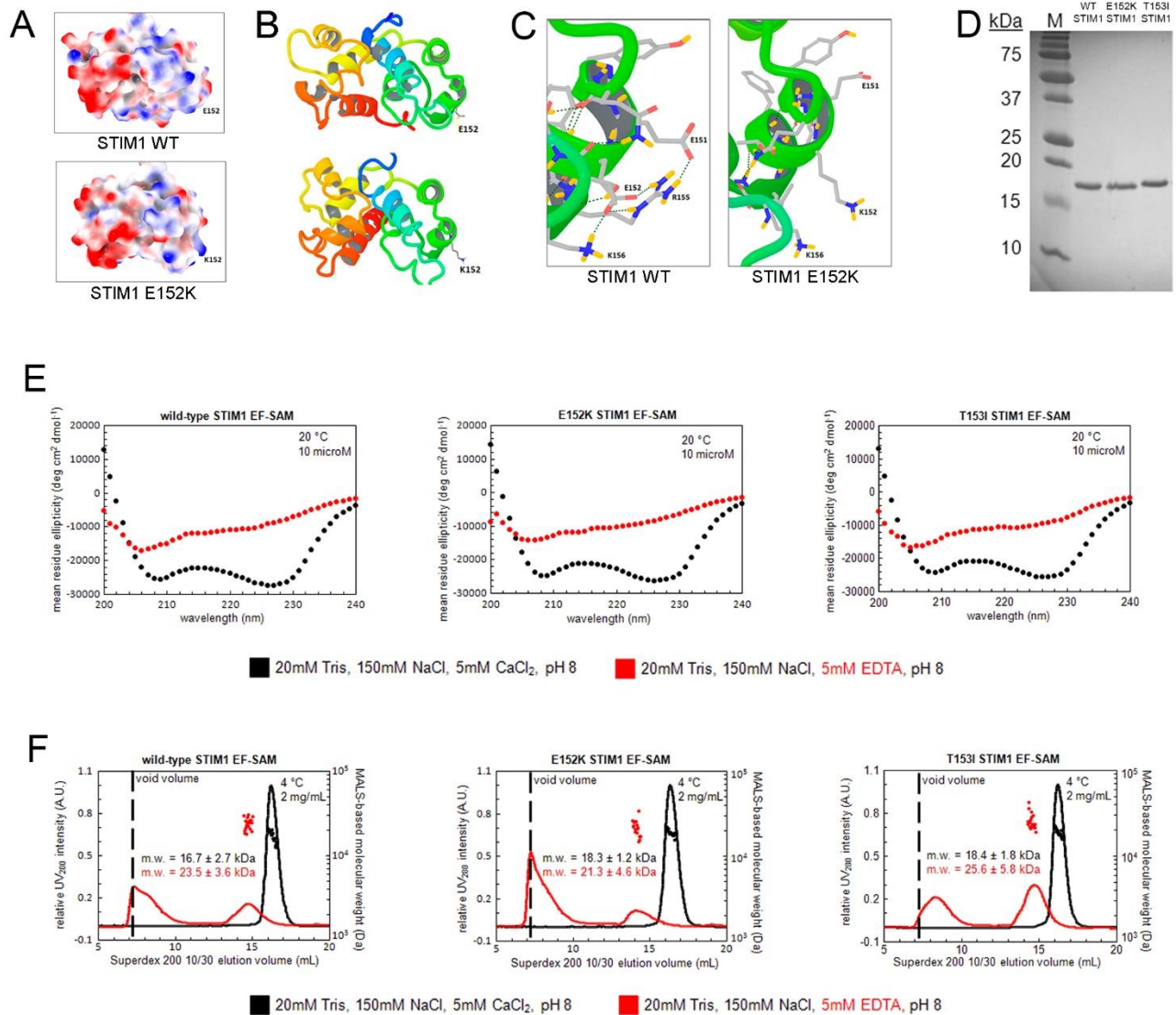


**Fig. S3.** (A), Molecular dynamics relaxation of human WT STIM1 and STIM1 E152K virtual structures containing residues 58-201 from human WT STIM1 protein (upper panel) and E152K variant (lower panel). Partial charges are shown on the surface depictions where red denotes negative charges, blue denotes positive charges and white is neutral. Note the faint red spot corresponding to E152 in the wild-type and the strong blue of K152 in the mutant. (B), WT STIM1 and STIM1 E152K structures: the EF-hand domain is shown as red, orange and yellow helices whereas the SAM domain is represented as green and blue helices. (C), Comparison of E152 and K152 interactions with neighboring residues. Left hand panel: E152 in the WT STIM1 exhibits consistent hydrogen bonding with neighboring K156 and R155 residues, extending to an interaction between R155 and E151. Right hand panel: K152 in the mutant human STIM1 extends independently outward from the protein as does K156 and E151 (and occasionally R155) without forming

hydrogen bonding, thereby providing a flexible cationic site in the SAM domain. **(D)**, Detection of purified EF-SAM domains of WT or mutated human STIM1 by Western blot. Coomassie blue-stained SDS-PAGE of WT and mutant (E152K and T153I) EF-SAM protein domains used in this study. 0.065 mg mL<sup>-1</sup> protein was loaded into each lane. **(E)**, Mutated EF-SAM domains retain the ability to sense Ca<sup>2+</sup> changes without differences referred to WT. Far-UV-CD spectra of WT and mutant EF-SAM purified domains. Data were acquired in the presence of 5mM CaCl<sub>2</sub> (black circles) or 5mM EDTA (red circles) at 20°C. Protein concentrations were 10 μM. **(F)**, SEC-MALS of WT and mutant EF-SAM purified domains. SEC elution profiles were generated in the presence of 5mM CaCl<sub>2</sub> (black lines) or 5mM EDTA (red lines) at 4°C using an S200 10/300 GL column. The vertical broken lines indicate the relative position of the column volume. The MALS molecular weights were determined in-line and are shown as black and red circles for the Ca<sup>2+</sup>-loaded and -depleted states, respectively, above the corresponding elution peaks. The average molecular weights ± S.D. are indicated on the plots. Protein concentrations were 2 mg mL<sup>-1</sup>. Buffers in **(E)**, and **(F)**, were 20mM Tris, 150mM NaCl, pH 8.

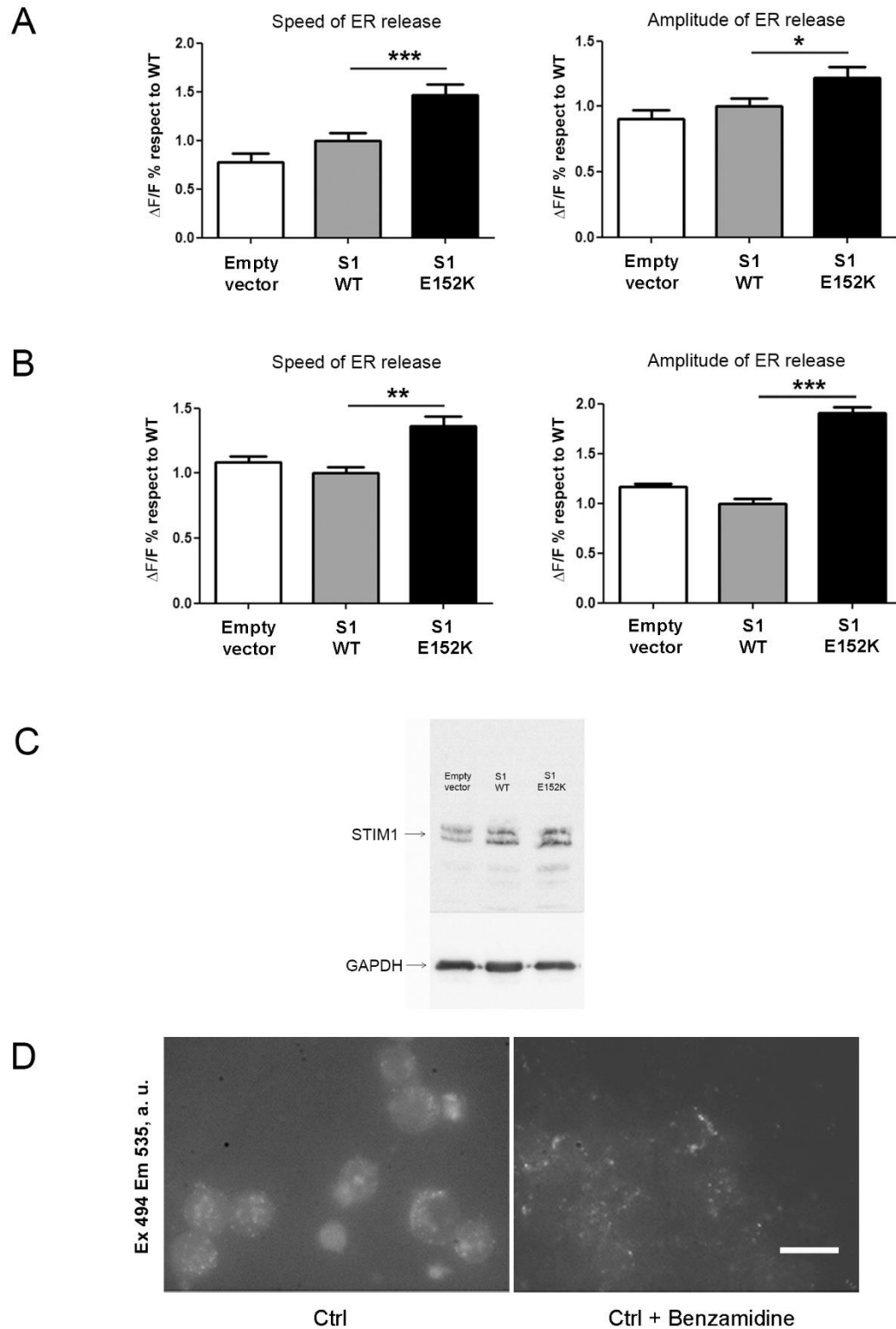


**Fig. S4. (A)**, Average values of the rate (left panel) and amplitude (right panel) of ER Ca<sup>2+</sup> release after 100 μM CCh treatment in the absence of extracellular Ca<sup>2+</sup>. n = 15 (empty vector), 14 (WT), 33 (E152K) **(B)**,

Average values of the rate (left panel) and amplitude (right panel) of ER Ca<sup>2+</sup> release after 2 μM thapsigargin treatment in the absence of extracellular Ca<sup>2+</sup> n = 135 (empty vector), 98 (WT), 82 (E152K). **(C)**, STIM1 expression in AR42J cells as revealed by Western blot for WT, E152K STIM1 or an empty vector. GAPDH was used as a loading control. **(D)**, Fluorescence images (excitation 494nm, emission 535 nm) showing a typical BZIPAR expression in non-treated cells (left image) and after benzamidine treatment (right image). Scale bar, 50 μM.